RESEARCH ARTICLE

Synthetic torpor in the rat protects the heart from ischaemia-reperfusion injury

Megan Elley[1]*, Ludovico Taddei[1,2], Muzammil Ali Khan[1], Una R Wilcox[1,3], Timna Hitrec[2], Martin Lewis[4], Anthony E Pickering[1], Michael Ambler[1]*

[1]Anaesthesia, Pain, and Critical Care Research Group, School of Physiology, Pharmacology, and Neuroscience, University of Bristol, Bristol, United Kingdom; [2]Department of Biomedical and Neuromotor Sciences, University of Bologna, Bologna, Italy; [3]Queen Mary University, London, United Kingdom; [4]Bristol Hospitals NHS Trust, Bristol, United Kingdom

eLife Assessment

This **important** submission from Ambler and colleagues brings new insights into how torpor conditions may confer resilience in cases of cardioprotection. The study is backed by **solid** evidence and represents a unique interoceptive mechanism of interest.

Abstract During times of environmental stress, many animals enter torpor: a reversible protective physiological state typically characterised by reductions in core temperature, heart rate, and oxygen consumption. Species that naturally enter this hypothermic and hypometabolic state are tolerant of ischaemia-reperfusion injury. Consequently, there is a growing interest in utilising aspects of torpor for clinical applications such as protection from stroke or myocardial infarction. It is currently unknown, however, whether a torpor-like state is protective in animals that do not naturally enter torpor. Using viral vector-mediated chemogenetic activation of the medial preoptic area of the hypothalamus, we induced synthetic torpor in the rat, a species that does not naturally enter torpor. We demonstrate this state is cardioprotective in an ex vivo ischaemia-reperfusion injury model with an ~40% reduction in infarct size. Synthetic torpor-induced cardioprotection of the normothermic, isolated heart is not dependent on prior hypothermia in vivo. Phosphoproteomic analysis of cardiac tissue indicates that the protective effects of synthetic torpor may be mediated by parallel activation of cell survival and stress tolerance pathways and inhibition of cell death pathways. These findings provide important insights into the mechanisms of organ protective effects of synthetic torpor states with implications for future clinical translation in humans.

***For correspondence:**
meg.elley@bristol.ac.uk (ME);
m.ambler@bristol.ac.uk (MA)

Competing interest: The authors declare that no competing interests exist.

Funding: See page 20

Preprint posted
07 January 2026
Sent for Review
03 March 2026
Reviewed preprint v1
08 July 2026
Reviewed preprint v2
25 September 2026
Version of Record
12 November 2026

Reviewing Editor: Moses V Chao, NYU Langone Health, United States

© Copyright Elley *et al*. This article is distributed under the terms of the Creative Commons Attribution License, which permits unrestricted use and redistribution provided that the original author and source are credited.

Introduction

Cardiovascular disease, including stroke and myocardial infarction, is the leading cause of death and disability globally (***Virani et al., 2021***; ***Murray et al., 2020***). Most current treatment strategies focus on re-establishing tissue perfusion, but there is interest in developing alternative strategies to improve tolerance to the ischaemia and/or reduce the impact of the reperfusion injury (***Zhang et al., 2024***). The idea that therapeutic hypothermia might reduce cell death during ischaemia-reperfusion has remained popular for many years, fuelled by encouraging animal studies (***Worp et al., 2010***; ***Leonov et al., 1990***; ***Chu et al., 2005***; ***Zhang et al., 2022***; ***Kyo et al., 2022***). However, despite early positive trials (***Nielsen et al., 2013***), more recent clinical data do not support the hypothesis that induced hypothermia improves outcomes following cardiac arrest (***Dankiewicz et al., 2021***). Failure to translate benefits from animal studies to adult clinical conditions may be due to side-effects arising from the

eLife digest A squirrel sleeping through winter is doing something remarkable: reducing its metabolism to a fraction of its normal rate, then switching it back on without damage. This state is called torpor – a reversible reduction in body temperature, heart rate and oxygen consumption that animals enter when energy is scarce. Hibernation is essentially a prolonged series of torpor bouts.

Animals in torpor have an unusual ability to withstand interruptions to their blood supply. This is particularly interesting for medicine because heart attacks and strokes damage tissue by depriving it of oxygen. Although mice do not hibernate throughout winter, they can enter torpor on a daily basis when they lack sufficient energy to keep themselves warm.

Recent studies have begun to unravel how the brain controls this process in mice, revealing that torpor is triggered by a small group of neurons in the hypothalamus, a brain region involved in regulating body temperature and appetite. Torpor occurs in a wide range of mammals, including some primates. This raises the question whether all mammals are able to enter torpor, and whether some have just stopped doing it. If so, could this dormant response be reawakened?

Until now, researchers had studied the protective effects of torpor only in animals that naturally enter this state. It was therefore unclear whether this protection is a specialised adaptation of hibernating animals or a more widely conserved biological mechanism. Elley et al. set out to investigate whether they could induce a torpor-like state in rats – which do not naturally enter torpor – by activating the equivalent brain cells. And, if so, whether this would protect their hearts from injury. The answer could help determine whether torpor research has potential relevance for human medicine.

To do this, the researchers used genetically engineered viruses to deliver instructions that enable targeted neurons to produce a new protein on their surface. This protein acts as a molecular switch, allowing us to activate the neurons using a drug. They found that stimulating neurons in the same hypothalamic region that triggers torpor in mice induced a convincing torpor-like state in rats. Their body temperature dropped to around 31°C, their heart rate fell by 24%, and their oxygen consumption decreased by 43%.

Elley et al. then examined whether this state protected the heart. Hearts removed from these rats and studied in isolation sustained around 40% less damage following a period without oxygen. Remarkably, this protection was still observed when they activated the same brain region but kept the rats warm, preventing their body temperature from falling. Further analysis of cardiac proteins revealed that pathways promoting cell survival had been activated, while those involved in cell death were suppressed.

This is early-stage laboratory research, and any potential benefit for patients remains a long way off. Ultimately, this work could have implications for people at risk of interrupted blood supply to their organs, including during heart attacks, strokes, cardiac arrest, organ transplantation and major surgery. Before this approach could be translated into medicine, however, researchers need to establish whether it can protect organs when activated after an injury has already begun, identify the signals the brain sends to the heart, and find a way to trigger these protective mechanisms using drugs.

counter-regulatory reflexes triggered by physical cooling. These reflexes lead to haemodynamic instability, shivering with increased oxygen consumption, cardiac arrhythmias, and electrolyte and glucose disturbances (***Dundee et al., 1953***; ***Sandestig et al., 2014***). Hence, interest is growing in centrally driven hypometabolic, hypothermic states that might avoid these counter-regulatory responses. With this in mind, researchers have turned to hibernating animals as a model for a centrally driven protective hypometabolic state (***Kyo et al., 2022***; ***Zancanaro et al., 1999***; ***Bolling et al., 1997***; ***Cerri, 2017***).

During hibernation, animals enter torpor, which is a remarkable physiological adaptation typically characterised by rapid and profound reductions in core temperature, heart rate, and oxygen consumption (***Ambler et al., 2021***). It serves as a protective adaptive response to relative energy deficit, achieved by a controlled reduction in metabolic demand in response to reduced availability of substrate. Torpor can be prolonged, in seasonal hibernators, or brief in daily heterotherms such as the mouse. During torpor, body temperature can be lowered to a few degrees above ambient temperature (***Swoap and Gutilla, 2009***; ***Heldmaier et al., 2004***). Metabolic activity may fall to below 5% of the euthermic rate, with active and profound decreases in cardiac output and minute ventilation, all of

which rapidly return to 'normal' values on arousal without harm to the individual (***Swoap and Gutilla, 2009***; ***Heldmaier et al., 2004***). Seasonal hibernators spend prolonged periods in a torpid state and are highly tolerant of ischaemia-reperfusion injury (***Zancanaro et al., 1999***; ***Bhowmick et al., 2017***; ***Jani et al., 2011***). This has motivated efforts to develop biomimetic torpor-like states for clinical applications that could provide a range of benefits, including protection from ischaemia-reperfusion injury (***Cerri, 2017***).

A fundamental hypothesis underlying interest in such translational torpor research is that conserved mechanisms exist in species that do not naturally enter torpor (potentially including humans), aspects of which might be harnessed to improve clinical outcomes. There are several reasons to suppose this to be the case. Firstly, torpor is extremely widespread, seen in all endothermic vertebrate classes, including primates (***Heldmaier et al., 2004***; ***Barnes and Carey, 2004***). Secondly, a unique torpor gene (or complement of genes) has so far not been described. Rather, those mammals that enter torpor do so through activation of ubiquitous genetic pathways (***Srere et al., 1992***; ***Faherty et al., 2016***; ***Zhao et al., 2010***). Thirdly, body temperature is not fixed even in 'strict' homeotherms: non-rapid-eye-movement sleep (NREM) is a controlled state of reduced body temperature and inactivity, features it shares with torpor (***Harding et al., 2018***; ***Zhang et al., 2015***).

Attempts to induce a 'synthetic' torpor-like state in a species for which it is not a natural behaviour have focused on the rat and include inhibition of the rostral ventromedial medulla (***Cerri et al., 2013***); peripheral infusion of drugs, such as adenosine and neurotensin analogues (***Zakharova et al., 2019***; ***Ferhat et al., 2025***); and targeted activation of neurons in the preoptic area of the hypothalamus (POA, ***Takahashi et al., 2020***). Of these approaches, the latter is arguably the closest to mimicking natural torpor, since it engages neurons in part of the hypothalamus that drives entry into natural torpor in mice (***Takahashi et al., 2020***; ***Hrvatin et al., 2020***; ***Zhang et al., 2020b***). We sought to

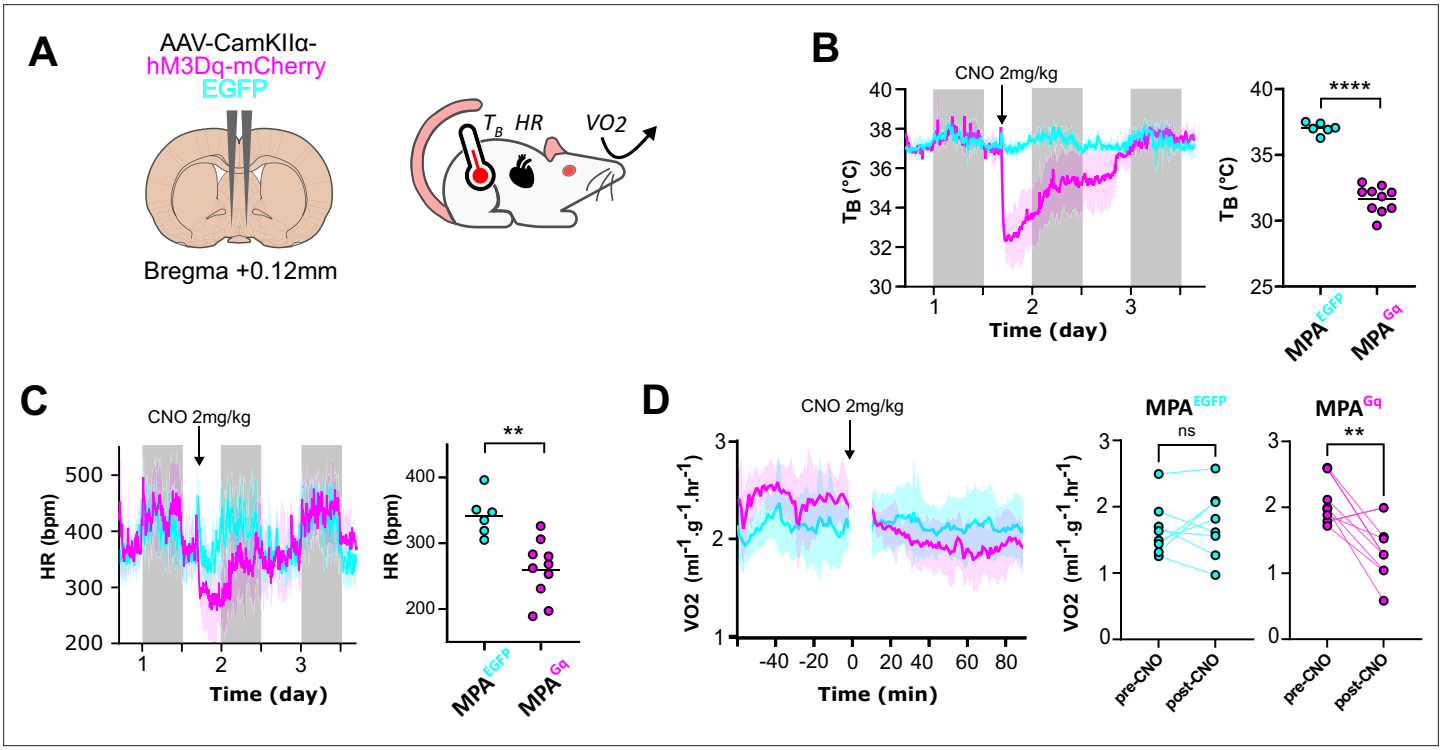

Figure 1. Chemogenetic activation of neurons in the medial preoptic area (MPA) induces synthetic torpor in the rat. Chemogenetic activation of neurons in the rat MPA (**A**) induces synthetic torpor characterised by reduced core body temperature (**B**, $F(3,24) = 106.4$, $p<0.0001$), bradycardia (**C**, $F(3,24) = 9.637$, $p=0.0002$), and reduced oxygen consumption (**D**, MPA^{GFP} $t(7) = 0.5655$, $p=0.5894$, MPA^{Gq} $t(7) = 4.305$, $p=0.0035$). For B and C, n=6 controls and 10 synthetic torpor, mean value for 90–100 min after CNO 2 mg/kg IP. For D, n=8 MPA^{GFP} and 8 MPA^{Gq} pre (50–60 min) vs post (120–130 min) CNO. Shaded area indicates SEM. * indicates $p<0.05$, ** indicates $p<0.01$, *** indicates $p<0.001$, **** indicates $p<0.0001$. Abbreviations: T_B, core temperature; VO_2, oxygen consumption; HR, heart rate; CNO, clozapine-N-oxide; ST, synthetic torpor; bpm, beats per minute.

The online version of this article includes the following figure supplement(s) for figure 1:

Figure supplement 1. Chemogenetic activation of medial preoptic area (MPA) neurons does not influence activity of rats.

characterise the state of synthetic torpor induced in the rat by targeted activation of neurons in the hypothalamic medial preoptic area (MPA) and to test the hypothesis that induction of synthetic torpor protects the heart from ischaemia-reperfusion injury.

Results

Induction of biomimetic synthetic torpor in the rat

We used viral vector-mediated chemogenetics to selectively activate neurons in the MPA (***Figure 1***, ***Figure 1—figure supplement 1***). The vector (AAV-CaMKIIa-hM3D(Gq)-mCherry) was injected bilaterally into the rat MPA, resulting in local expression of the modified receptor hM3Dq (a Gq-coupled Designer Receptor Exclusively Activated by Designer Drug [DREADD]; ***Armbruster et al., 2007***; ***Roth, 2016***) under the control of the CaMKIIα promoter (***Basu et al., 2008***; ***Egashira et al., 2018***) (producing MPA^{Gq} rats). Control animals underwent identical procedures but received injection of AAV-CaMKIIa-EGFP into the MPA, which results only in the expression of a green fluorescent protein (MPA^{EGFP} rats).

Subsequent MPA neuronal activation using intraperitoneal CNO (2 mg/kg) induced a rapid and reversible decrease in core temperature (mean temperature post-CNO in MPA^{Gq} rats 31.64 ± 1.02°C vs MPA^{EGFP} rats 37.05 ± 0.43°C, p<0.0001, see ***Figure 1B***). This was accompanied by a 24% lower heart rate (mean heart rate post-CNO in MPA^{Gq} rats 260±44 bpm vs MPA^{EGFP} 342±32 bpm, p<0.005, ***Figure 1C***). This was also associated with a 39% reduction in oxygen consumption in MPA^{Gq} rats (mean oxygen consumption prior to CNO 2.08±0.34 ml/g/hr vs 1.29±0.42 ml/kg/hr post-CNO, p=0.0035, ***Figure 1D***). Whereas there was no significant change in oxygen consumption in MPA^{EGFP} rats (mean oxygen consumption prior to CNO 1.25±0.4 ml/g/hr vs 1.68±0.62 ml/g/hr post-CNO, p=0.589, ***Figure 1D***). Hence, chemoactivation of neurons in the rat MPA produces a synthetic torpor state that recapitulates three key features of natural torpor: hypothermia, bradycardia, and reduced oxygen consumption.

Mapping the distribution of the neurons responsible for synthetic torpor in the rat

We mapped the location of mCherry-expressing transduced neurons within the anterior hypothalamus of six animals (***Figure 2***, ***Figure 2—figure supplement 1***). We observed transduced neurons in a region stretching from bregma +0.12 mm to –0.48 mm, spreading 1 mm bilaterally from the midline, and from the ventral surface of the hypothalamus to 1.5 mm dorsally (***Figure 2F***). This region includes the targeted MPA, as well as more caudal regions of the preoptic area, such as the medial preoptic nucleus.

Characterising the neurons in the rat MPA responsible for inducing synthetic torpor

To establish whether the neurons involved in inducing this synthetic torpor state are excitatory or inhibitory, we used in situ hybridisation (ISH) to examine colocalisation of vector-mediated mCherry expression (***Figure 2A–E***) with genes that encode vesicular glutamate transporter 2 (*Vglut2*, gene ID *Sl17a6*) and vesicular GABA transporter (*Vgat*, gene ID *Slc32a1*) (***Figure 2B***). We found a large proportion of transduced neurons expressed *Vglut2* (72%, ***Figure 2D***). We also detected a population of transduced neurons that co-express both *Vglut2* and *Vgat* (35%), termed 'dual-phenotype' neurons (***Ottem et al., 2004***; ***Figure 2D***). A small proportion of vector-transduced neurons were inhibitory (14%), expressing *Vgat*, while the remainder expressed neither *Vglut2* nor *Vgat* (15%) (***Figure 2D***).

Previous studies have identified a population of neurons within the preoptic area of the mouse hypothalamus, which can integrate stimuli to regulate thermogenesis and metabolism and induce a torpor-like state upon activation (***Upton et al., 2021***). These stimuli include temperature changes both locally within the hypothalamus and from peripheral signals in the skin, inflammatory prostaglandin signalling, leptin, oestrogen, and violet light. These neurons were called QPLOT neurons, reflecting their co-expression of neuropeptide pyroglutamylated RFamide peptide (Qrfp), prostaglandin EP3 receptor (encoded by *Ptger3*), leptin receptor (encoded by *Lepr*), violet light-sensitive opsin, neuropsin (encoded by *Opn5*), and neurokinin B (encoded by *Tacr3*). Consequently, we sought to determine whether the neurons responsible for inducing synthetic torpor in the rat share similarities

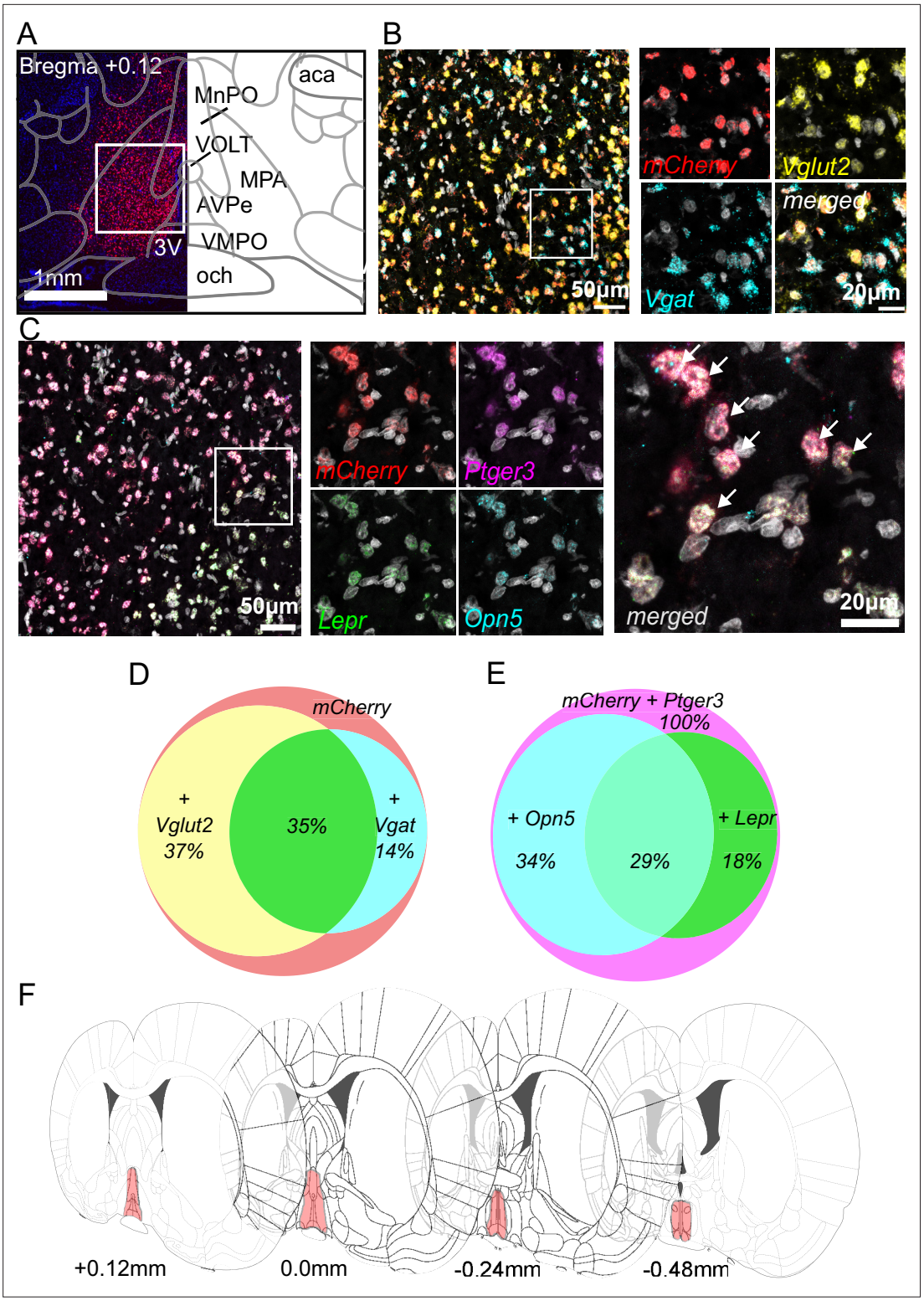

Figure 2. Characterisation of neurons in the rat MPA responsible for inducing synthetic torpor. (**A**) Viral vector transduction with mCherry in the MPA (red) and corresponding anatomical schematic. (**B**) RNA in situ hybridisation labelling vector-transduced cells (mCherry, red), and those expressing *Vglut2* (yellow) and/or *Vgat* (turquoise). (**C**) RNA in situ hybridisation labelling vector-transduced cells (mCherry, red), and those expressing *Ptger3* (purple), *Lepr* (green), and *Opn5* (turquoise). White arrows indicate transduced cells that express *Ptger3*, *Lepr*, and *Opn5*. (**D**) Co-expression of *Vglut2* and *Vgat* amongst transduced cells. (**E**) Expression of QPLOT markers amongst vector-transduced cells (note all transduced cells expressed *Ptger3*). (**F**) Schematic showing extent of viral vector transduction common to all animals. Abbreviations: MPA, medial preoptic area; MnPO, median preoptic

Figure 2 continued on next page

Figure 2 continued

nucleus; VOLT, vascular organ of the lamina terminalis; 3V, third ventricle; AVPe, anteroventral periventricular nucleus; VMPO, ventromedial preoptic nucleus; och, optic chiasm; aca, anterior commissure (anterior part); *Vglut2*, vesicular glutamate transporter 2; *Vgat*, vesicular GABA transporter; *Ptger3*, prostaglandin EP3 receptor; *Lepr*, leptin receptor; *Opn5*, opsin-5.

The online version of this article includes the following figure supplement(s) for figure 2:

Figure supplement 1. mCherry viral vector mapping demonstrating the transduction throughout the rat brain.

to this torpor-inducing population identified in mice. We again used ISH to assess colocalisation of vector-expressed mCherry with three markers of QPLOT neurons: *Ptger3*, *Lepr*, and *Opn5*. We found 100% of the virally transduced cells also expressed *Ptger3* (***Figure 2D and E***). Additionally, 34% of these mCherry and *Ptger3* positive neurons also expressed *Opn5*, 18% co-expressed *Lepr* (***Figure 2E***), and 29% of mCherry-positive neurons were positive for all three of the five QPLOT neuron markers we labelled (***Figure 2E***). These findings suggest a degree of conservation of neuronal organisation within the MPA between mice and rats and are consistent with synthetic torpor being produced by activation of analogous 'torpor-generating' circuits across species.

Induction of synthetic torpor protects the heart from ischaemia-reperfusion injury

Both hypothermia (***Kuczynski et al., 2019***) and torpor (***Zancanaro et al., 1999***; ***Bhowmick et al., 2017***; ***Jani et al., 2011***) have been shown to protect against ischaemia-reperfusion injury. We therefore sought to test the effects of synthetic torpor on tolerance to cardiac ischaemia-reperfusion injury in the ex vivo Langendorff isolated heart preparation (***Bell et al., 2011***; ***Figure 3A***). Induction of synthetic torpor, 90 min prior to removal of the heart for the Langendorff preparation and exposure to ischaemia-reperfusion, reduced infarct size by 39.5% (percentage infarcted myocardium: MPA^{Gq} 18.7±9.6% vs MPA^{EGFP} 30.9 ± 9.1%, p=0.039, ***Figure 3B and C***). Importantly, although the synthetic torpor state reduced the body temperature of the rats prior heart excision, the perfusion of warm Krebs-Henseleit Buffer (KHB) to the cardiac tissue for a 30 min stabilisation period ensured that there were no differences in temperature at the time of ischaemia and reperfusion.

To examine whether the synthetic torpor-induced myocardial protection depends upon the preceding hypothermia, we housed groups of MPA^{Gq} and MPA^{EGFP} rats at a thermoneutral temperature of 28–30°C. Administration of CNO to MPA^{Gq} rats under thermoneutral conditions prevented the drop in core temperature that was observed in recordings at room temperature (p<0.0001, see ***Figure 3D***, ***Figure 3—figure supplement 1***). Furthermore, comparing thermoneutral MPA^{Gq} rats with room temperature MPA^{EGFP} control rats showed no significant temperature change (mean temperature post-CNO in thermoneutral MPA^{Gq} rats 36.4 ± 0.73°C vs MPA^{EGFP} 37.05 ± 0.43°C, p=0.44, ***Figure 3D***). However, the bradycardia observed with synthetic torpor induced at room temperature persisted even when rats were housed at a thermoneutral temperature (***Figure 3E***). A 21% lower heart rate was observed in the thermoneutral MPA^{Gq} compared to MPA^{EGFP} rats (mean heart rate post-CNO in thermoneutral MPA^{Gq} rats 298±43 bpm vs thermoneutral MPA^{EGFP} rats 379±62 bpm, p<0.05, see ***Figure 3E***, ***Figure 3—figure supplement 1***). This indicates that the heart rate changes associated with synthetic torpor were not secondary to the induced hypothermia. Additionally, there were no significant differences in the heart rate of animals in the MPA^{EGFP} condition compared to the thermoneutral MPA^{EGFP} condition (p=0.53, ***Figure 3E***) or between the MPA^{Gq} and thermoneutral MPA^{Gq} condition (p=0.38, ***Figure 3E***, ***Figure 3—figure supplement 1***).

We found that thermoneutral synthetic torpor still reduced the infarct size (percentage infarct in the thermoneutral MPA^{Gq} rats 9.6 ± 8.4% compared to thermoneutral MPA^{EGFP} rats 36.2 ± 23.5%, p=0.005 and room temperature MPA^{EGFP} rats, p=0.007, ***Figure 3C***). There were no significant differences in infarct size between the MPA^{Gq} and thermoneutral MPA^{Gq} groups (p=0.31) nor between the MPA^{EGFP} and thermoneutral MPA^{EGFP} groups (p=0.38) (***Figure 3C***). We also found no correlation between individual nadir temperature during synthetic torpor and infarct size (p=0.3714, R^2=0.089, ***Figure 3—figure supplement 2***). These findings indicate that the myocardial protection conferred by synthetic torpor is independent of the hypothermia.

Heart rate was monitored during the Langendorff assay to test for the possibility that the bradycardia observed in vivo during synthetic torpor persisted in the ex vivo cardiac preparation and

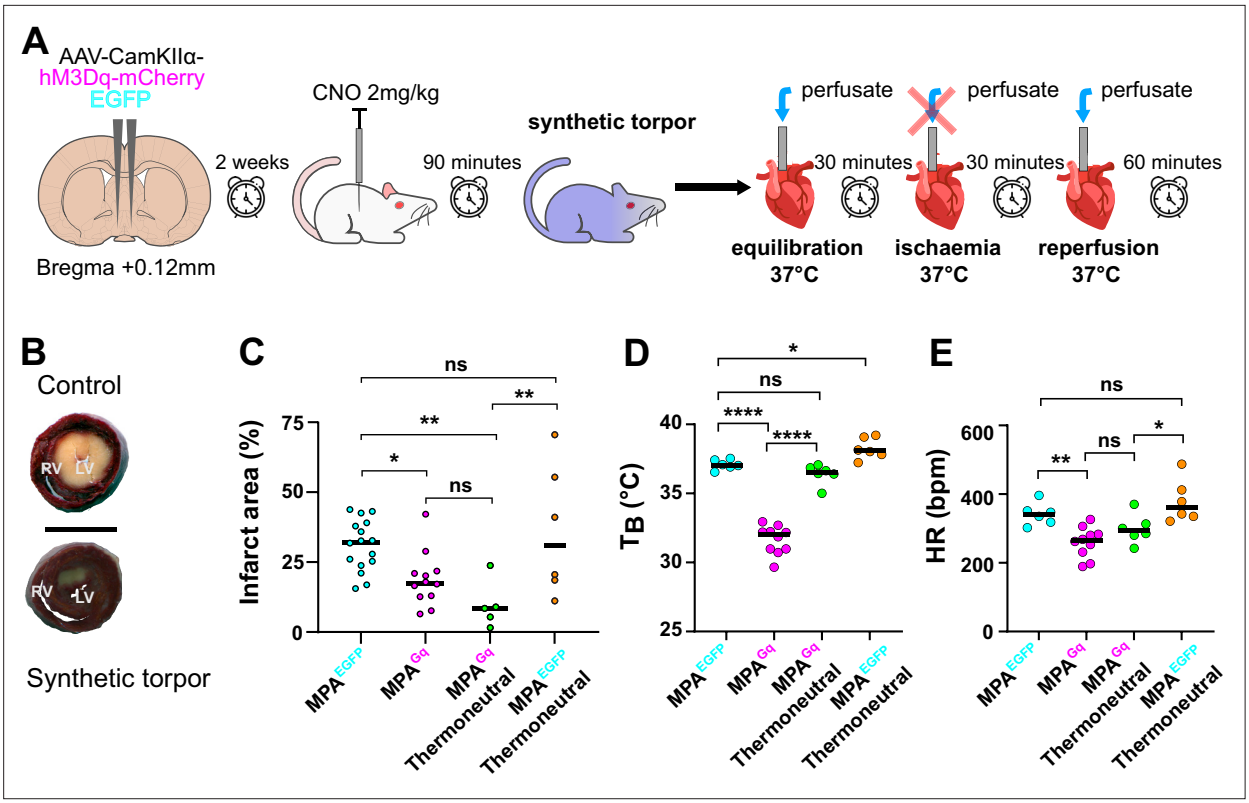

Figure 3. Synthetic torpor protects the heart from ex vivo ischaemia-reperfusion injury. Rats first underwent bilateral injection of vector (hM3DGq or GFP) into the medial preoptic area (MPA). After 2 weeks, they all received CNO, inducing synthetic torpor in rats that had received hM3DGq vector, followed by removal of the heart and ischaemia-reperfusion in the Langendorff preparation (**A**). Pre-conditioning with synthetic torpor resulted in significantly reduced infarct size as measured by 2,3,5-triphenyltetrazolium chloride (TTC) staining. (**B, C**). Scale bar represents 1 cm. For C, controls (n=16), torpor (n=12), thermoneutral synthetic torpor (n=5), and thermoneutral controls (n=6). This cardioprotective effect was not dependent on a reduction in core temperature as rats held at a thermoneutral ambient temperature following CNO injection were still protected (**C**, analysis of variance [ANOVA], F(3,35)=6.542, p=0.0013) MPA^{EGFP} compared to MPA^{Gq} p=0.039 and thermoneutral MPA^{EGFP} compared to thermoneutral $MPAG^{qp}$ = 0.007. Inducing synthetic torpor in a thermoneutral environment prevented the drop in core temperature (**D**, F(3,24) = 106.4. p<0.0001), but not the bradycardia (**E**, F(3,24) = 9.637, p=0.0002). Holm-Sidak correction for multiple comparisons. Data shown is median and IQR. For D and E, MPA^{EGFP} (n=6), MPA^{Gq} (n=10), MPA^{Gq} thermoneutral (n=6) and MPA^{EGFP} thermoneutral (n=6), mean value for 90–100 min after CNO 2 mg/kg IP *=p<0.05, **=p<0.01, ****=p<0.00001, ns = p>0.05. Abbreviations: CNO, clozapine-N-oxide; RV, right ventricle; LV, left ventricle; T_B, core temperature; HR, heart rate; bpm, beats per minute.

The online version of this article includes the following figure supplement(s) for figure 3:

Figure supplement 1. Pre-Langendorff in vivo physiological changes (**A, B**) and ex vivo heart rates (**C**).

Figure supplement 2. Relationship between nadir surface body temperature during synthetic torpor and cardiac infarct size.

hence contributed to the myocardial protection. No differences were observed in heart rates during the 30 min equilibration period (prior to induction of ischaemia) in MPA^{Gq} (240±28 bpm), MPA^{EGFP} (248±23 bpm), thermoneutral MPA^{Gq} (225±20 bpm), and thermoneutral MPA^{EGFP} (225±21 bpm) conditions, F(3,19) = 1.35, p=0.29 (***Figure 3—figure supplement 1C***). This indicates the decreased heart rate observed during synthetic torpor in vivo does not persist ex vivo.

Phosphoproteomic analysis of cardiac tissue following synthetic torpor

To further understand the mechanisms underlying the cardioprotective effect observed in synthetic torpor, we conducted mass spectrometry (MS) using tandem mass tag (TMT) which allowed us to analyse the phosphoproteomic profile of rat heart tissue following 90 min of synthetic torpor (without ischaemia-reperfusion injury exposure) compared to control rats. After quality control and preprocessing, we identified 4064 phosphopeptides from 1090 unique genes in our rat samples. Missingness, inter-sample correlation, principal component analysis (PCA) distance, and phosphosite distributional properties did not identify any outlier samples (***Figure 4***, ***Figure 4—figure supplements 1 and 2***).

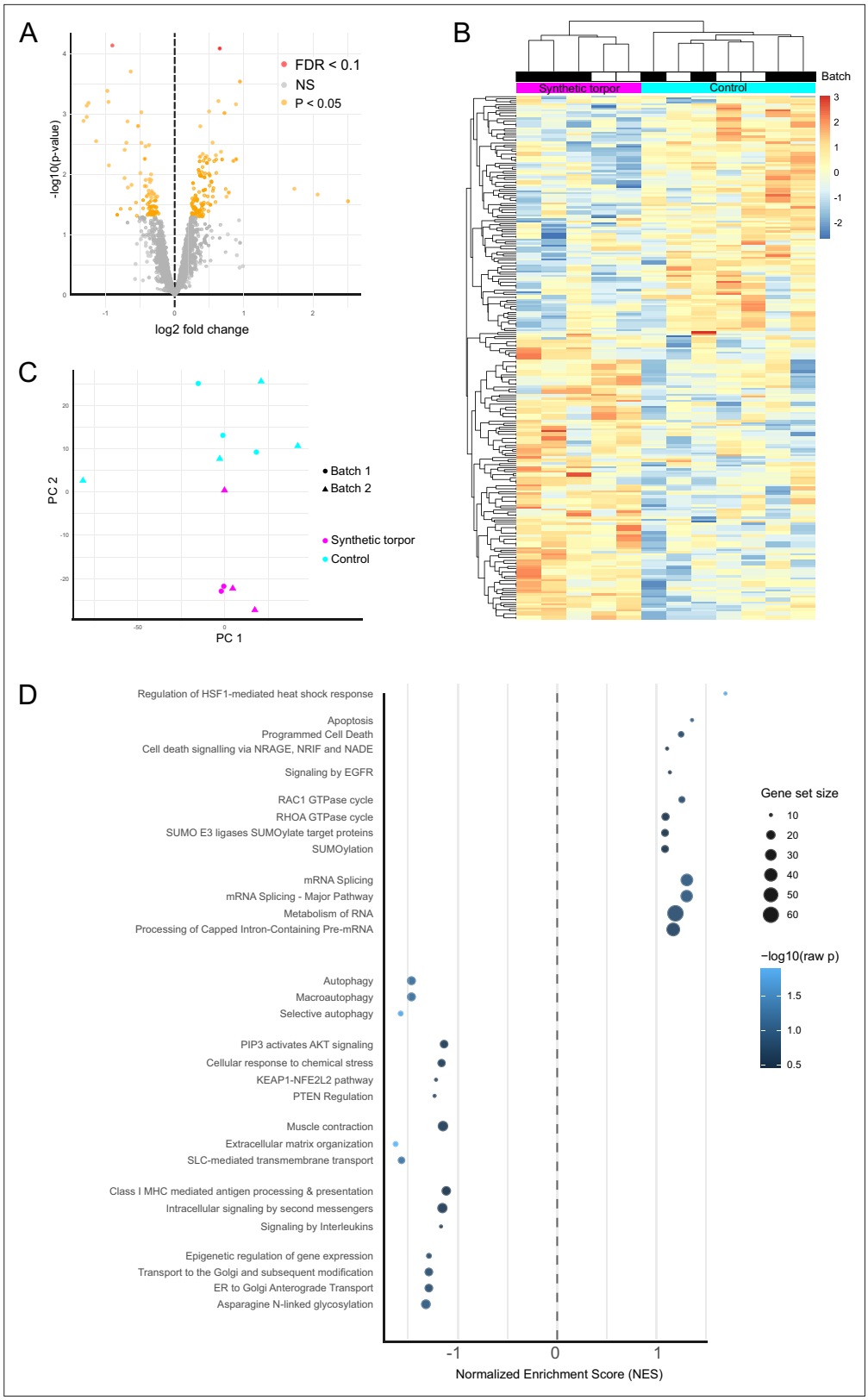

Figure 4. Phosphoproteome analysis of the heart identifies gene pathways associated with synthetic torpor. Volcano plot showing differentially expressed phosphopeptides after limma modelling (**A**). Heatmap shows the top 300 differentially expressed phosphosites between synthetic torpor (n=5) and controls (n=7) after limma modelling. Rows (phosphosites) and columns (sample) clustered by similarity of expression, such that phosphopeptides that

Figure 4 continued on next page

Figure 4 continued

covary cluster together, as do samples with similar expression profiles (**B**). Principal component analysis confirms group separation and effective batch correction (**C**). Gene level set enrichment analysis (GSEA) performed using a single representative phosphosite per gene (selected based on limma t-statistic) identifies key pathways modulated by entry into synthetic torpor (**D**).

The online version of this article includes the following figure supplement(s) for figure 4:

Figure supplement 1. Phosphoproteomics workflow.

Figure supplement 2. Proteomics QC metrics.

The purpose of this analysis was exploration and hypothesis generation and therefore the results were not corrected for multiple comparisons (***Figure 4***).

We analysed the proteomics data in two parallel and complementary ways. One approach collapsed the phosphosite data from multiple potential sites to a single site per protein, with representative sites selected by limma (***Ritchie et al., 2015***) t-statistic for the most differentially enriched between synthetic torpor and controls. The corresponding gene for each protein (1073) and the associated t-statistic was then used as the input for gene set enrichment analysis (GSEA) using ReactomePA (***Yu and He, 2015***), which returned 136 differentially enriched pathways. GSEA performed in this way on phosphoproteome data is agnostic to the direction of modulation (i.e. while a negative enrichment score indicates relative dephosphorylation of the representative phosphosite, GSEA does not impute the effect this will have on the pathway in terms of increasing or decreasing activity). We focused on the top 30 most differentially enriched pathways. This analysis revealed a coordinated ensemble of pathway modulation involving control of apoptosis and autophagy, cellular stress response mechanisms, control of transcription and translation, and regulation of heat shock proteins (***Figure 4***).

The second approach reconstructed rat phosphoprotein structure from phosphopeptides, mapped them to human orthologues via their corresponding gene (***Durinck et al., 2009***; ***Pagès et al., 2025b***), and then performed post-translational modification set enrichment analysis (PTM-SEA). This approach,

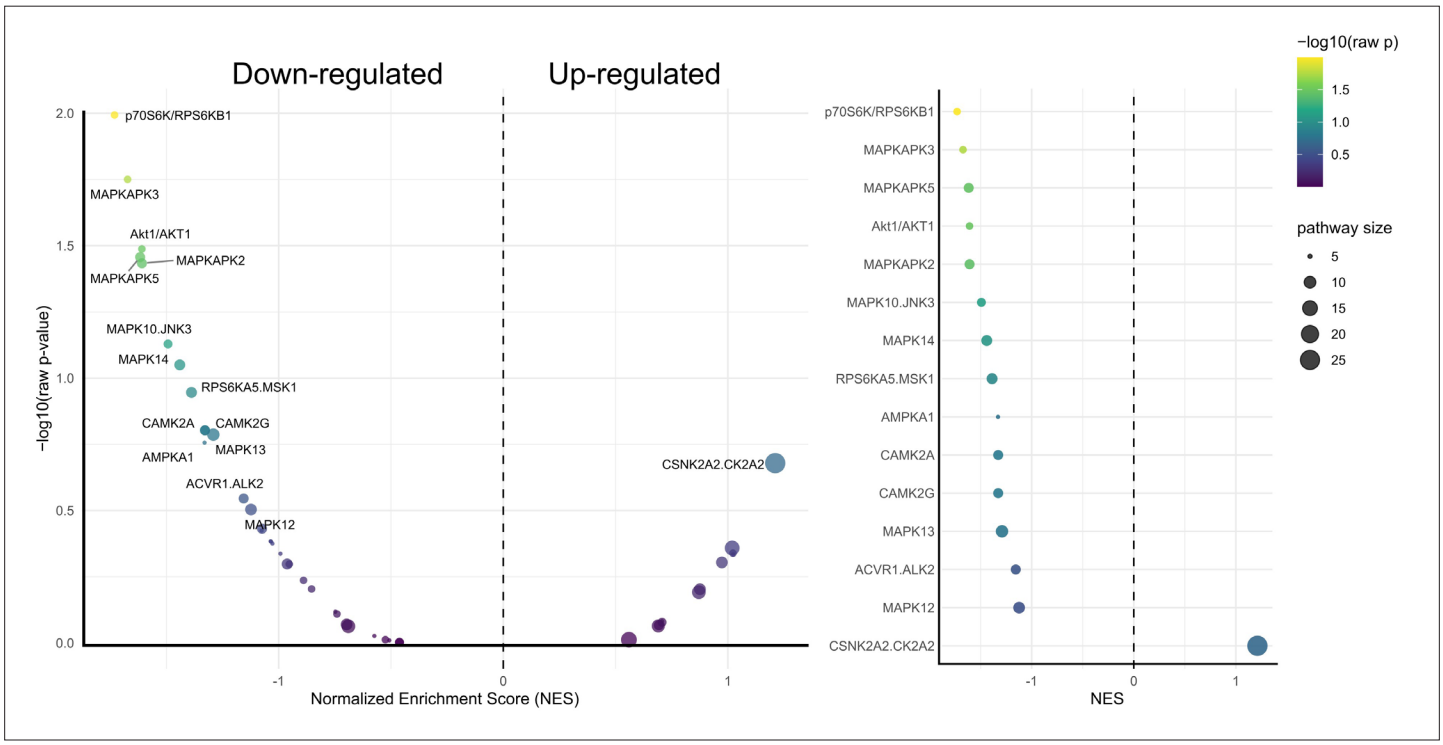

Figure 5. Site-level phosphoproteome analysis. After mapping from rat to human phosphoproteins, post-translational modification set enrichment analysis (PTM-SEA) was performed on 1384 aligned phosphosites from 595 rat gene-human protein pairs. Kinase signatures are shown ranked by normalised enrichment score (NES); the top 15 by absolute NES are labelled for clarity. Colour represents $-\log_{10}$(raw p-value), and point size indicates pathway size.

by retaining site-specific phosphorylation state data, identifies key kinases by the signature pattern of phosphorylation changes across the analysed proteome, in this case returning whether the kinase has been activated or inhibited. We were able to fully map 1384 phosphosites from 595 proteins from our rat sample to corresponding human phosphoproteins. This is necessary because the rat phosphoproteome is less well studied and the PTM-SEA package is based on human data (***Korotkevich et al., 2016***). We found 156 differentially enriched kinase signatures across the 1384 phosphosites. We focused on the 15 most differentially enriched kinase signatures (***Figure 5***). Again, we saw a coordinated ensemble of kinase modulation by synthetic torpor, including suppression of mTOR-Akt-ribosomal growth signalling indicating reduced anabolic drive (reduced Akt, p70S6K, RPS6KA5); dampened stress-activated MAPK pathways (MAPK12–14 and MAPKAPK2, 3, and 5); downregulated excitability (reduced activity of MAPK10, CAMK2A, and CAMK2G); reduction of cellular energy consumption (reduced AMPKα1); and reduced growth/hypertrophy (reduced ACVR1 activity). In parallel, we saw increased activity of CSNK2A2, suggesting increased stress tolerance and cytoprotection. Hence, both gene-level pathway analysis and specific kinase enrichment analysis indicate that synthetic torpor invokes a coordinated pattern of protective adaptations.

Discussion

We implemented a chemogenetic model of synthetic torpor in the rat (***Takahashi et al., 2020***), a species that does not naturally enter torpor, by targeting a population of hypothalamic neurons analogous to those that drive fasting-induced torpor in the mouse. We demonstrate that synthetic torpor in the rat is strongly cardioprotective in an ex vivo ischaemia-reperfusion injury model, even in the absence of hypothermia. In parallel, phosphoproteome analysis revealed changes consistent with enhanced cellular stress tolerance and inhibition of cell death pathways, which may contribute to the observed cardioprotection. Importantly, because synthetic torpor was induced in a species that does not naturally enter torpor, these findings support the existence of conserved, cross-species mechanisms that could potentially be translated for therapeutic use in humans.

Recent years have seen a resurgence of interest in torpor and torpor-like states, driven by a hope that aspects of this remarkable physiology could be mimicked in both clinical and space-flight situations. Here, we demonstrate that chemogenetic activation of neurons in the MPA of a non-torpid species, the rat, recapitulates three main features of natural torpor: hypothermia (***Figure 1B***), bradycardia (***Figure 1C***), and reduced oxygen consumption (***Figure 1D***). Interestingly, we did not observe a significant reduction in the motor activity of the rats during synthetic torpor (***Figure 1—figure supplement 1***), which is typically observed in mice during both natural and synthetic torpor (***Hrvatin et al., 2020***). The POA is a key centre for control of energy balance, body temperature, and as a driver of natural fasting-induced torpor in the mouse (***Hrvatin et al., 2020***; ***Takahashi et al., 2020***; ***Ambler et al., 2022***; ***Saper and Machado, 2020***). Analysis of pooled single-nucleus RNA sequencing data has attempted to phenotype the critical neuronal population, from which emerge 'QPLOT neurons' (***Hrvatin et al., 2020***; ***Upton et al., 2021***; ***Moffitt et al., 2018***). These cells express QRFP (***Takahashi et al., 2020***), prostaglandins E3 receptor (EP3) (***Machado et al., 2020***), leptin receptor (***Yu et al., 2016***), the violet light-sensitive receptor Opn5 (***Zhang et al., 2020a***), and neurokinin 3 receptors (encoded by *Tacr3*) (***Padilla et al., 2018***). Expression of two or more of these markers is considered sufficient to identify neurons from this population (***Upton et al., 2021***). 81% of the neurons we targeted with the DREADD viral vector expressed either two or three of these QPLOT neuron markers (***Figure 2C and E***). And 29% of these neurons expressed all three markers used, which included *Ptger3, Lepr,* and *Opn5* (***Figure 2C and E***). The observation that virally transduced cells in the rat MPA also express QPLOT markers indicates the presence of a neuronal population in rats with expression patterns and physiological effects equivalent to those described in mice, supporting the existence of a conserved, cross-species population.

We found that 72% of transduced mCherry neurons were positive for *Vglut2*, a marker of excitatory neurons (***Figure 2B and D***). Of these neurons, 35% were labelled as 'dual-phenotype' (***Ottem et al., 2004***), expressing markers of both excitatory and inhibitory neurons (*Vglut2* and *Vgat*, ***Figure 2B and D***). This was anticipated, as we used viral vector-mediated chemogenetics under the control of the CamKIIα promoter, which targets excitatory neurons (***Basu et al., 2008***; ***Egashira et al., 2018***), but with some tropism for inhibitory neurons also (***Veres et al., 2023***). Furthermore, a subset of neurons involved in mouse torpor express both excitatory and inhibitory RNA markers (***Takahashi et al., 2020***).

Whether these neurons functionally release glutamate and GABA remains to be seen, but evidence in the rat suggests that while EP3 receptor-expressing thermoregulatory neurons in the preoptic area may express excitatory and inhibitory markers, they are functionally inhibitory (***Nakamura et al., 2022***).

A key question that emerges from the observation of synthetic torpor in the rat is: what is the natural role of these neural circuits and why do they not naturally induce torpor in response to fasting? EP3 receptor-expressing neurons in the rat POA have been implicated in bidirectional control of body temperature (***Nakamura et al., 2022***). These neurons are inhibited by prostaglandins to produce fever and activated by warmth exposure to reduce body temperature. It is likely that these neurons and the population we have identified overlap. Hence, rats might maintain the capacity to activate these neurons in response to rising ambient temperature (and inhibit them in response to prostaglandins) but no longer be able to activate them in response to fasting. Alternatively, the rat may engage these neurons to reduce temperature at sleep onset (***Alföldi et al., 1990***), but may have lost the ability to engage them to the extent that the animal enters torpor. Torpor and sleep may be functionally linked: mice enter and emerge from torpor through NREM sleep (***Huang et al., 2021***) and the MPA of the hypothalamus appears to be responsible for triggering natural torpor (***Takahashi et al., 2020***; ***Hrvatin et al., 2020***; ***Ambler et al., 2022***), as well as the cooling associated with NREM sleep onset (***Harding et al., 2018***; ***Zhang et al., 2015***).

Animals that were pre-conditioned with 90 min of synthetic torpor showed a 40% smaller infarct size compared to control animals (***Figure 3***). These findings support prior studies in species known to naturally enter torpor. For example, seasonal hibernators in torpor are highly tolerant of ischaemia-reperfusion injury in multiple organs, including kidney and intestines (***Zancanaro et al., 1999***; ***Bhowmick et al., 2017***; ***Jani et al., 2011***; ***Kurtz et al., 2006***); inducing a torpor-like state using deep brain stimulation (DBS) to stimulate the MPA in mice is neuroprotective in a brain ischaemia model (***Zhang et al., 2022***); and targeting RFP-amide-expressing neurons in the MPA to trigger a torpor-like state ameliorates acute kidney injury (***Zhang et al., 2022***; ***Kyo et al., 2022***) following ischaemia-reperfusion. Until now, this work was all carried out in species known to naturally enter torpor (mice and ground squirrels) and so it was not clear whether other species might also benefit from an induced torpor-like state. Our study demonstrates for the first time that inducing a torpor-like state in a species (the rat) that does not naturally enter torpor is protective in a cardiac ischaemia-reperfusion injury model.

This study utilised an ex vivo model of ischaemia-reperfusion injury in the Langendorff preparation. Our finding that activation of MPA EP3-expressing neurons in the rat was cardioprotective indicates that activity in this neuronal population induces changes in the cardiac tissue that persist when the heart is isolated from the rest of the organism. Whether the protective signal in vivo is circulating or released locally via vagal efferents remains an important question. The bradycardia we observed in vivo in response to chemoactivation of neurons within the MPA still occurs in the absence of hypothermia (***Figure 3E***, ***Figure 3—figure supplement 1B***), suggesting active suppression of heart rate via the cardiac vagus nerve. Importantly, bradycardia did not persist during the ex vivo Langendorff preparation (***Figure 3—figure supplement 1C***). This was important to assess, as lower heart rate in the Langendorff assay has previously been shown to decrease the size of the infarcted tissue area (***Delgado-Betancourt et al., 2023***). Hence, our model of synthetic torpor appears to engage protective responses that persist in isolation and are neither temperature-dependent nor driven by a simple reduction in the heart rate during ischaemia-reperfusion.

Strikingly, chemogenetic activation of MPA neurons under thermoneutral conditions (which prevented hypothermia) still reduced infarct size. This was established by the thermoneutral condition, which prevented any decrease in core body temperature while the animals were in synthetic torpor (***Figure 3D***) yet still resulted in a significant decrease in myocardial infarction size compared to control (***Figure 3C***). We also observed no correlation between individual nadir surface temperature during synthetic torpor and the infarct size (***Figure 3—figure supplement 2***). These data show that the hypothermic component of torpor is not necessary for the protective effects of synthetic torpor. There have so far been mixed findings regarding the necessity for a drop in temperature to observe protection. One study used DBS or chemogenetics to activate neurons within the mouse MPA to drive a torpor-like state and found that hypothermia is required for neuroprotection in a stroke model (***Zhang et al., 2022***). In contrast, and similar to our present study, Kyo and colleagues demonstrated that the hypothermic element of a torpor-like state in the mouse is not required to reduce acute

kidney injury in response to ischaemia (***Kyo et al., 2022***). Torpor-induced reduction in core temperature might be sufficient to improve tolerance to ischaemia-reperfusion injury, but some models (our present study and that of ***Kyo et al., 2022***) might engage additional, temperature-independent protective responses.

To explore the potential mechanisms occurring at the cardiac cellular level during synthetic torpor, we analysed the phosphoproteome of hearts taken from animals in synthetic torpor. We found many differentially regulated phosphoproteins and enrichment of numerous pathways associated with cell stress response, cell cycle, and death (***Figure 6***). The PTM-SEA data (***Figure 5***) suggests activation of CSNK2A2 in response to synthetic torpor, a protein kinase associated with promoting cell survival, DNA repair, and inhibition of apoptosis (***Borgo et al., 2021***). A number of kinases were also inhibited, including Akt and p70S6K, which are associated with the mTOR signalling pathway (***Saxton and Sabatini, 2017***). mTOR signalling is implicated in metabolic regulation, and a decrease in activity of this pathway indicates reduced anabolism (***Saxton and Sabatini, 2017***), which is also observed in calorie restriction (***Ham et al., 2025***) (a known natural driver of daily torpor; ***Wheatley et al., 2025***) and altered mTOR signalling is also seen in deep hibernating animals such as ground squirrels (***Chang et al., 2020***; ***Wu and Storey, 2012***). Inhibiting mTOR signalling protects against myocardial ischaemia-reperfusion injury by regulating autophagy and limiting cardiomyocyte apoptosis (***Das et al., 2012***; ***Duan et al., 2024***). Decreased AMPK signalling is also indicative of a shift in cellular metabolism, playing an integral role in coordinating autophagy and mitochondrial function (***Herzig and Shaw, 2018***).

Several MAPK kinases were inhibited during synthetic torpor, including MAPK10/JNK3, MAPK12-14, and downstream MAPKAPK2 (MK2), MAPKAPK3 (MK3), and MAPKAPK5 (MK5). MAPK signalling is fundamental for cell survival, inflammation, and regulating apoptosis. Cell stress, apoptosis, and inflammation are strongly associated with ischaemia-reperfusion injury, and several studies have demonstrated that pharmacological inhibition of p38 MAPK pathway reduced cardiac remodelling and infarct size post myocardial infarction injury (***Muslin, 2008***). Altered MAPKs have been reported in deep hibernation (***Childers et al., 2019***; ***Eddy and Storey, 2007***), supporting the hypothesis that synthetic torpor in the rat is analogous to natural torpor/hibernation.

Tightly regulated calcium signalling within the heart is crucial for muscle contraction and maintaining a regular heart rhythm. Excessive CAMKII activation is linked to dysregulated calcium signalling, myocardial dysfunction, and electrical instability (***Swaminathan et al., 2012***). Furthermore, in ischaemia-reperfusion injury, there is a disruption to calcium signalling during ischaemia, followed by overload on reperfusion, leading to mitochondrial dysfunction and cell death (***Bertero et al., 2024***). Here, we demonstrate downregulated activity of CAMKIIA and CAMKIIG kinases, which is typically associated with improved contractility and reduced cell death in models of heart disease (***Swaminathan et al., 2012***; ***Zhang et al., 2005***). Changes to calcium handling and CAMKII signalling have also been observed in mammalian hibernators (***Brauch et al., 2005***; ***Xie et al., 2021***). We also demonstrated a reduction in ACVR1 activity. ACVR1 is thought to mediate the development of cardiac hypertrophy, and blocking this signalling pathway reduces pathological cardiac remodelling (***Shahid et al., 2016***).

These findings are also consistent with the GSEA reactome data (***Figure 4***), with modulation of pathways associated with cell stress and survival (such as PI3/AKT/mTOR, MAPK, and calcium signalling) and cell cycle and death (such as autophagy and apoptosis). We hypothesise that the activation of MPA neurons within the rat hypothalamus drives changes in a network of pathways within the cardiac tissue that synergistically contribute to the cardioprotective effect of synthetic torpor (***Figure 6***).

Limitations

These experiments were conducted in an ex vivo Langendorff model of ischaemia-reperfusion injury. While we have no reason to suppose that similar protection would not be observed in vivo, we have not explicitly tested this. Synthetic torpor was applied prior to the ischaemia-reperfusion injury; it remains to be seen whether synthetic torpor applied after reperfusion can modulate the injury. Our phosphoproteome analysis was exploratory and hypothesis-generating due to relatively small numbers of samples and the high demands of false discovery rate (FDR)-corrected statistics when analysing thousands of phosphopeptides. The POA is enriched with oestrogen receptors (***Moffitt et al., 2018***) and previous work by our group has demonstrated that the estrous cycle modulates fasting-induced

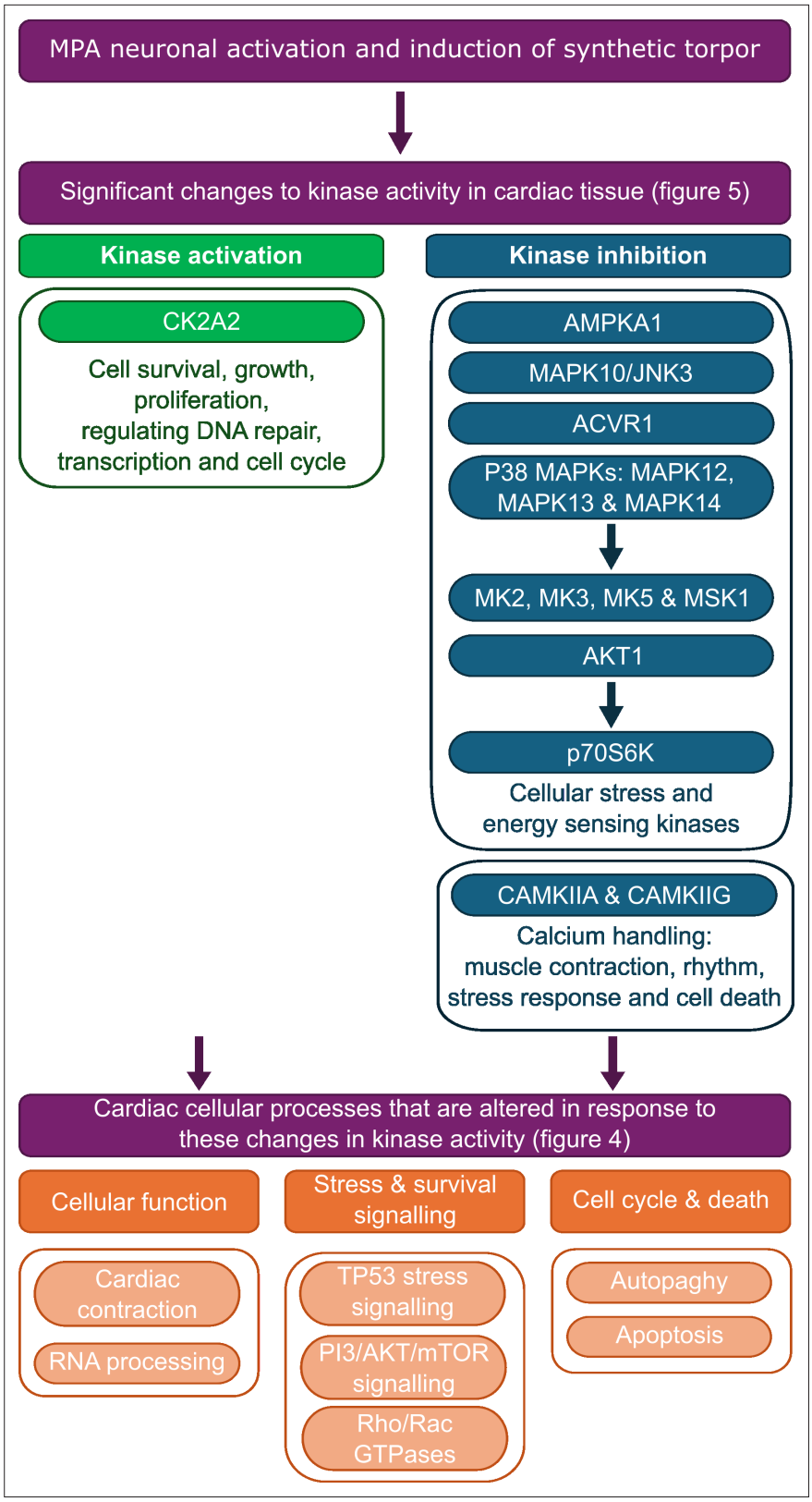

Figure 6. Changes to phosphoproteome signature that drive cardioprotection in synthetic torpor. Synthetic torpor induction by medial preoptic area (MPA) neuronal activation induces changes to kinase signatures in cardiac tissue which are associated with cell survival/stress, cell cycle/death, and cellular function. Activated kinases are shown in green and inhibited kinases in blue. Arrows indicate kinases that act downstream of the ones above. Abbreviations:

Figure 6 continued on next page

Figure 6 continued

CK2A2, casein kinase II alpha II subunit; AMPKA1, AMP-activated protein kinase alpha 1; MAPK10/JNK3, mitogen-activated protein kinase 10/c-Jun N terminal kinase; ACVR1, activin A receptor type 1; MAPK12/13/14, mitogen-activated protein kinase 12/13/14; MK2/3/5, mitogen-activated protein kinase-activated protein kinase 2/3/5; AKT1, AKT serine/threonine kinase 1; p70S6K, 70 kDa ribosomal protein s6 kinase; CAMKIIA/G, calcium/calmodulin-dependent protein kinase II A/G; TP53, tumour protein p53; PI3K, phosphoinositide 3-kinase; mTOR, mechanistic target of rapamycin.

torpor (***Marshall et al., 2026***). Our current work did not aim to investigate sex differences and is not powered to include this analysis. It should also be noted that the effect on oxygen consumption was not assessed in the thermoneutral synthetic torpor animals and we consequently cannot say whether a reduction in metabolic rate occurred in these animals.

Our study represents an important step towards harnessing torpor and synthetic torpor states for clinical translation. We have shown that species that do not naturally enter torpor can be induced to do so through targeted activation of neuronal populations that correspond to those responsible for natural torpor in the mouse. This state of synthetic torpor confers protection from ischaemia-reperfusion independent of body temperature or heart rate, and which persists in the isolated heart. It adds to a growing body of evidence that the central nervous system is able to induce protective adaptations in the heart (***Haykin et al., 2024***; ***Machhada et al., 2020***; ***Mastitskaya et al., 2012***).

Methods

Rats

All studies had the approval of the local University of Bristol Animal Welfare and Ethical Review Board and were conducted in accordance with the UK Animals (Scientific Procedures) Act. Male and female Wistar rats (175–250 g) were obtained from Charles River and were housed at 21°C on a 12 hr light/dark cycle with ad lib access to food and standard rat chow (LabDiet).

Viral vectors

AAV-CaMKIIa-hM3D(Gq)-mCherry was a gift from Bryan Roth (Addgene viral prep # 50476-AAV5) and was used at a titre of 1.7×10^{13} viral genome copies per ml. AAV-CaMKIIa-EGFP was also a gift from Bryan Roth (Addgene viral prep # 50469-AAV5) and was used at a titre of 2.8×10^{13} viral genome copies per ml.

Stereotaxic injection of viral vectors

Rats were anaesthetised with intraperitoneal injection of ketamine (5 mg/100 g, Vetalar; Pharmacia) and medetomidine (30 µg/100 g Domitor, Pfizer) until loss of paw withdrawal reflex. Additional intraperitoneal injections of anaesthetic were administered as needed to maintain surgical depth of anaesthesia. Core temperature was maintained using a servo-controlled heat pad and a rectal temperature probe (Harvard Apparatus). The planned incision site was shaved, the skin was cleaned with iodine solution, and sterile surgical technique was used throughout. Anaesthetised rats were placed in a stereotaxic frame, the head was fixed in atraumatic ear bars, and skull position maintained by an incisor bar (David Kopf Instruments). Microcapillary pipettes were made from microcapillary glass (Sigma) on a vertical pipette puller (Harvard Apparatus). Pipettes were filled with mineral oil; then vector was back-filled using a robotic microinjector (Nano-W wireless capillary microinjector, Neurostar), producing a visible vector-mineral oil interface. The scalp was incised in the midline and burr holes made bilaterally with a drill attachment (Neurostar). Bilateral injections were made at depths of 8.5 mm relative to the surface of the brain, +0.12 mm from Bregma, and 0.4 mm from the midline. Each injection was 200 nl and was delivered at a rate of 100 nl/min. The injection pipette remained in place for 5 min after the injection before slowly removing. Following vector injections, the wound was closed with non-absorbable suture and dressed with antibacterial wound powder. Anaesthesia was reversed with atipamezole (1 mg/kg i.p., Antisedan, Zoetis), and meloxicam analgesia given subcutaneously (5 mg/kg, Metacam, Boehringer Ingelheim). Rats were recovered in a heated chamber, then housed separately for 3 days following surgery and monitored daily.

Implantation of telemeters

During the anaesthesia for stereotaxic CNS injections, a subset of rats was additionally implanted with telemetric temperature and electrocardiogram (ECG) probes into the abdomen (DSI ETA-F10 implant, Data Science International, Harvard Bioscience Inc). A vertical incision was made through the skin in the abdomen just below the xiphisternum approximately 2–3 cm in length and a smaller incision made to the skin at the right-hand side of the chest, for placement of the ECG electrode. Telemeter wires were passed under the skin and sewn into place using non-absorbable sutures. An intraperitoneal incision was made into the abdomen for placement of the telemetry implant, which was closed with absorbable sutures. Finally, the skin incisions were closed with non-absorbable sutures and dressed with antibacterial wound powder. Anaesthesia was reversed with atipamezole (1 mg/kg i.p., Antisedan, Zoetis), and meloxicam analgesia given subcutaneously (5 mg/kg, Metacam, Boehringer Ingelheim). Rats were recovered in a heated chamber, then housed separately for 3 days following surgery, and monitored daily.

Induction of synthetic torpor

Intraperitoneal injection of clozapine-N-oxide dihydrochloride (CNO), a synthetic ligand that activates the DREADD $hM3D_q$ (2 mg/kg, Tocris Bioscience, #6329), was used to induce synthetic torpor. For those rats that were not implanted with telemeters, synthetic torpor induction was confirmed using thermal imaging with a FLIR C2 camera. Synthetic torpor was defined by a drop in core temperature below 35°C in telemetered animals, or surface temperature below 30°C in thermally imaged animals following CNO injection. Some MPA HM3DGq viral injections failed and animals did not enter synthetic torpor; the success rate for inducing synthetic torpor was 80%, so consequently 20% of the animals were excluded from the study.

Telemetric monitoring of core body temperature, ECG, and motor activity

Telemetry implants were switched on and connected to a receiver platform (DSI PhysioTel receiver RPC-1, Data Science International, Harvard Bioscience Inc). Continuous telemetry data, including core body temperature, ECG, and motor activity were acquired and recorded wirelessly using DSI Matrix 2.0 (MX2, Data Science International, Harvard Bioscience Inc) and Ponemah software (Ponemah v6.00, Data Science International, Harvard Bioscience Inc). Recordings were made from animals in their home cages for data at room temperature. For the thermoneutral condition, maintaining control rats in an ambient temperature of 30°C caused them to become hyperthermic, hence 28°C was used for these animals, while MPA^{Gq} rats remained euthermic at 30°C following CNO injection. Post recording, ECG, temperature, and activity data were filtered to remove noise and analysed in Ponemah software. The R wave component of the ECG recordings was detected and used to determine the heart rate in bpm.

For some animals, surface body temperature in place of implanted telemetry was used to confirm entry into synthetic torpor. To do this, rats were moved into a custom built Perspex 32×42×56 cm^3 cage, and surface body temperature was recorded using an infrared thermal imaging camera placed above the cage (FLIR C2, https://www.flir.co.uk).

Measurement of oxygen consumption

Indirect calorimetry was performed using a CaloBox (Phenosys) (***Heldmaier et al., 2024***), with a gas flow rate of 75 l per hour and a sampling rate of 0.25 Hz. Rats were first acclimated to the recording chamber for 30 min over 3–5 days before undergoing CNO injection. Data was discarded for 10 min following CNO injection to allow the CaloBox to re-equilibrate. Food and water were available throughout the recording session.

Ex vivo model of cardiac ischaemia-reperfusion injury

90 min post CNO administration, an intraperitoneal injection of heparin was delivered (1000 IU, Sigma-Aldrich, #H3393). Animals were deeply anaesthetised with isoflurane (5%), which was delivered in a constant flow of oxygen (2 l/min). Following loss of pedal reflex, animals were sacrificed by cervical dislocation. A thoracotomy was performed and beating hearts were removed by sectioning the aorta. Hearts were quickly placed into ice-cold KHB (containing 120 mM NaCl, 25 mM $NaHCO_3$, 11 mM glucose, 1.2 mM KH_2PO_4, 1.2 mM $MgSO_4$, 4.8 mM KCl, and 1.2 mM $CaCl_2$). The aorta was

then cannulated (secured into place using suture threads) and hearts were perfused by the Langendorff method (Langendorff, 1898) on an isolated heart system apparatus. Hearts were perfused with carbonated KHB, maintained at 37°C, at a rate of 10 ml/min. ECG was continuously recorded by Ag electrodes placed near the apex of the heart. After a 30 min stabilisation phase, the hearts were then subjected to 30 min of global ischaemia, whereby perfusion was stopped, and hearts were submerged into a water-jacketed bath of KHB held at 37°C. After ischaemia, the hearts were reperfused for 60 min (***Figure 2A***). Exclusion criteria for experiments included time between excision of the heart and start of ex vivo perfusion with KHB of more than 2 min, more than two aortic cannulation attempts, and heart rate under 200 bpm at the end of the equilibration period. A total of eight animals were excluded based on these criteria.

Heart infarction assessment

Following 60 min of reperfusion, the hearts were perfused with 2.3.5-triphenyltetrazolium chloride (TTC) (Phytotech, USA) to demarcate infarcted tissue (unstained by TTC) and viable tissue (stained by TTC) (***Fishbein et al., 1981***). 1% TTC solution at 37°C was perfused through the aortic cannula at a rate of 2 ml/min and then hearts were submerged in 1% TTC for a further 15 min at 37°C, before being fixed in 4% paraformaldehyde (PFA) for 24 hr at 4°C. Hearts were then transversally sliced into 3-mm-thick sections, and each side of the sections were imaged using a flatbed scanner. ImageJ (NIH, USA) was used to outline and calculate the infarcted area and whole heart area (excluding ventricular chambers). Both infarcted and viable areas were averaged across each side for each heart section and infarct area was expressed as a percentage dividing total infarcted area by whole heart area. The assessor was blinded to the animal group.

Mapping of virally transfected MPA hypothalamic neurons

Immunofluorescence

Brains were extracted and post-fixed for 48 hr with 4% PFA at 4°C and then incubated in PBS with 30% sucrose and 0.03% sodium azide for a further 48 hr. Brains were embedded in tissue freezing medium and sectioned on a freezing microtome into 40 µm coronal sections and adhered to SuperFrost Plus slides (Epredia). A hydrophobic barrier was drawn around each slide using an ImmEdge Pen (Vector Laboratories) and allowed to dry at room temperature for 15 min. Sections were washed three times for 5 min in PBS and then blocked with 0.25% bovine serum albumin (BSA) and 10% normal donkey serum (NDS) in 0.3% Triton X-100 PBS (PBS-T) for 4 hr at room temperature. They were then incubated with primary antibody (anti-mCherry, 1:2000 dilution, BioVision, #5993) diluted in 0.25% BSA and 2% NDS in PBS-T overnight at room temperature. Slides were then washed three times for 5 min in PBS, followed by incubation with the secondary antibody (Alexa Fluor 594 donkey anti-rabbit, 1:1000 dilution, Abcam, #A-21207) diluted in 0.25% BSA in PBS-T for 4 hr at room temperature. Finally, slides were washed three times for 5 min in PBS and mounted with Fluoroshield with DAPI (Sigma-Aldrich).

Epifluorescence imaging and mapping

Sections were imaged using a Leica DM4000B widefield microscope with a ×20 magnification 0.5 numerical aperture objective, with a 515–561 nm excitation filter, dichroic mirror 580 nm, and a 590 nm emission filter. The anatomical extent of virally transduced cells was mapped independently by two individuals and agreed by consensus using the Allen Brain Atlas as reference.

Characterisation of neurons driving this torpor-like state

Fluorescence ISH

Brains were extracted and immediately frozen in 2-methylbutane and stored at –80°C until use. Brains were embedded in tissue freezing medium (Cryomatrix, Thermo Fisher) and sliced on a cryostat into 20 µm coronal sections, adhered to SuperFrost Plus slides (Epredia), and stored at –20°C overnight before undergoing the standard RNAscope Fluorescent Multiplex Assay for fresh frozen tissue (ACD Bio, Biotechne).

For the RNAscope ISH, mounted sections were fixed in 4% PFA for 15 min at room temperature, then dehydrated in increasing concentrations of ethanol (50%, 75%, then 100%) for 5 min in each. Sections were left overnight in a second application of 100% ethanol. Two sections per animal were selected for processing based on mCherry expression within the MPA and underwent one of two

Table 1. RNAscope probes used for in situ hybridisation (ISH).

Target	Protocol	Gene (entrez gene ID)	Species (homology*)	*Catalogue number (channel)*
VGLUT2	*1*	*Slc17a6 (84487)*	*Rat*	*317011 (C4)*
VGAT	*1*	*Slc32a1 (22348)*	*Mouse (97.6%)*	*319191 (C1)*
Prostaglandin E2 receptor (EP3)	*2*	*Ptger3 (249290)*	*Rat*	*586251 (C4)*
Leptin receptor	*2*	*Lepr (24536)*	*Rat*	*415951 (C2)*
Opn5 receptor	*2*	*Opn5 (353344)*	*Mouse (96.4%)*	*438071 (C1)*
mCherry	*1* and *2*	mCherry	*n/a*	*431201 (C3)*

*https://rddc.tsinghua-gd.org/.

protocols, protocol 1: markers of excitatory and inhibitory neurons and protocol 2: markers that have been associated with neurons controlling mouse torpor (see ***Table 1*** for probes used). Dehydrated sections were air-dried for 10 min at room temperature, treated with hydrogen peroxide for 10 min at room temperature, washed with distilled water, and then treated with protease IV for 12 min. The RNAscope probes were then applied to each slide and left to hybridise for 2 hr at 40°C in a humidified chamber. Following hybridisation, slides were washed with wash buffer twice for 2 min at room temperature. AMP1 was applied to each slide and left to incubate in a humidified oven for 30 min at 40°C, then washed again twice for 2 min. This amplification process was repeated for AMP2 and AMP3. Next, slides were washed twice with wash buffer for 2 min at room temperature and HRP-C1 was applied to sections for 15 min at 40°C in a humidified chamber. Slides were rinsed again with wash buffer for 2 min at room temperature and an Opal dye was incubated on the slides for 30 min at 40°C in a humidified chamber. Following this, slides were washed with wash buffer for 2 min at room temperature and the HRP blocker was applied to sections for 15 min at 40°C in a humidified chamber. This process was repeated for HRP-C2, C3, and C4 with different Opal dyes for each. Finally, the sections were rinsed in wash buffer for 2 min at room temperature and coverslipped with fluoroshield with DAPI and left to dry at room temperature overnight, before being stored at 4°C.

Confocal imaging

Brains were processed as indicated in 'Fluorescence ISH' section and imaged within 2 weeks of processing. Sections containing MPA were imaged on a Leica SP8 AOBS confocal laser scanning microscope attached to a Leica DMi8 inverted epifluorescence microscope using HyD detectors ('hybrid' SMD GaAsP detectors) with 405 nm diode and white light lasers. A 40× oil immersion lens with NA of 1.3 was used (HC PL APO CS2 lens). Tiled MPA images were taken and stitched using LASX software (Leica) and channels were imaged sequentially to avoid optical crosstalk.

ISH image analysis

Images were z projection compressed in ImageJ. A 50-pixel radius rolling ball background subtraction was applied to each image. An automated image processing pipeline was used to count DAPI- and RNA-positive nuclei. An Otsu threshold was applied to the DAPI image, and overlapping nuclei were separated using the watershed method. Cell nuclei were then filtered by size (20–200 μm^2) and counted and ROIs for each cell nuclei were saved in ImageJ. ROIs and cell identities created from the DAPI image were then overlaid on the ISH images and cell nuclei positive for RNA were counted. A minimum of 200 cells from each brain section were manually assessed to determine a threshold for nuclei positive for the different RNA transcripts, and these thresholds were then applied to the remaining cells.

Proteomics

Tissue preparation

90 min post CNO administration, animals were deeply anaesthetised with isoflurane (5%) delivered in a constant flow of oxygen (2 l/min) and sacrificed by cervical dislocation following loss of pedal reflex. A thoracotomy was performed and beating hearts were removed by sectioning the aorta. Hearts were quickly placed into ice-cold cardioplegia buffer (7.4 pH, containing 20 mM HEPES, 15 mM glucose, 15 mM KCl, 7.8 mM $MgSO_4$, and 1.2 mM $CaCl_2$) and agitated to remove blood. Hearts were then immersed and immediately frozen in 2-methylbutane in liquid nitrogen and stored at –80°C until use. For protein sample preparation, hearts were thawed gently on ice, and 50–100 mg sample was cut from the apex of each heart and placed into 10 µL of RIPA buffer and homogenised (3×15 s bursts at 10,000 RPM). Samples were then centrifuged at 10,000×*g* for 10 min at 4°C. Supernatant was transferred into a new tube and protein concentration was determined with the BCA Protein Assay Kit. Protein samples were diluted to a final concentration of 2 mg/ml in RIPA buffer and stored at –80°C.

TMT labelling, high pH reverse-phase chromatography, and phosphor-peptide enrichment

Protein samples were analysed using MS using TMT (Proteomics Facility, University of Bristol). Aliquots of 100 µg of each sample were digested with 2.5 µg trypsin at 37°C overnight and labelled with TMT (TMTpro) 16-plex reagents, and the labelled samples were then pooled.

For total proteome analysis, an aliquot of 100 µg of the pooled sample was desalted using a SepPak cartridge (Waters). Eluate from the SepPak cartridge was evaporated and resuspended in buffer A (20 mM ammonium hydroxide, pH 10) prior to fractionation by high pH reversed-phase chromatography using an Ultimate 3000 liquid chromatography system (Thermo Fisher Scientific). Briefly, the sample was loaded onto an XBridge BEH C18 Column (130 Å, 3.5 µm, 2.1 mm × 150 mm, Waters, UK) in buffer A and peptides eluted with an increasing gradient of buffer B (20 mM ammonium hydroxide in acetonitrile, pH 10) from 0% to 95% over 60 min. The resulting fractions (concatenated into 20 in total) were evaporated to dryness and resuspended in 1% formic acid prior to analysis by nano-LC MS/MS using an Orbitrap Fusion Lumos mass spectrometer (Thermo Scientific).

For phosphoproteome analysis, the remainder of the TMT-labelled pooled sample was also desalted using a SepPak cartridge and eluate evaporated and then subjected to TiO_2 enrichment according to the manufacturer's protocol. The flow-through and washes from the TiO_2-based enrichment were then subjected to FeNTA-based phosphopeptide enrichment according to the manufacturer's instructions (Pierce). The phospho-enriched samples were again evaporated to dryness and then resuspended in 1% formic acid prior to analysis by nano-LC MS/MS.

Nano-LC MS

High pH RP fractions (total proteome analysis) or the phospho-enriched fractions (phosphoproteome analysis) were further fractionated using an Ultimate 3000 nano-LC system in line with an Orbitrap Fusion Lumos mass spectrometer.

Peptides in 1% (vol/vol) formic acid were injected onto an Acclaim PepMap C18 nano-trap column (Thermo Scientific). After washing with 0.5% (vol/vol) acetonitrile, 0.1% (vol/vol) formic acid, peptides were resolved on a 500 mm×75 µm Acclaim PepMap C18 reverse-phase analytical column (Thermo Scientific) over a 150 min organic gradient, using seven gradient segments in solvent B (aqueous 80% acetonitrile in 0.1% formic acid) (gradients: 1–6% over 1 min, 6–15% over 58 min, 15–32% over 58 min, 32–40% over 5 min, 40–90% over 1 min, held at 90% for 6 min and then reduced to 1% over 1 min) with a flow rate of 300 nl/min. Peptides were ionised by nano-electrospray ionisation at 2.0 kV using a stainless-steel emitter with an internal diameter of 30 µm (Thermo Scientific) and a capillary temperature of 300°C.

All spectra were acquired using an Orbitrap Fusion Lumos mass spectrometer controlled by Xcalibur 3.0 software and operated in data-dependent acquisition mode using an SPS-MS3 workflow. FTMS1 spectra were collected at a resolution of 120,000, with an automatic gain control (AGC) target of 200,000 and a max injection time of 50 ms. Precursors were filtered with an intensity threshold of 5000, according to charge state (to include charge states 2–7) and with monoisotopic peak determination set to peptide. Previously interrogated precursors were excluded using a dynamic window (60 s±10 ppm). The MS2 precursors were isolated with a quadrupole isolation window of 0.7 m/z.

ITMS2 spectra were collected with an AGC target of 10,000, max injection time of 70 ms, and CID collision energy of 35%.

For FTMS3 analysis, the Orbitrap was operated at 50,000 resolution with an AGC target of 50,000 and a max injection time of 105 ms. Precursors were fragmented by high energy collision dissociation at a normalised collision energy of 60% to ensure maximal TMT reporter ion yield. Synchronous Precursor Selection (SPS) was enabled to include up to 10 MS2 fragment ions in the FTMS3 scan.

Data processing

The raw data files were processed and quantified using Proteome Discoverer software v2.4 (Thermo Scientific) and searched against the UniProt Rat database (downloaded July 2025: 47,902 entries) using the SEQUEST HT algorithm. Peptide precursor mass tolerance was set at 10 ppm, and MS/MS tolerance was set at 0.6 Da. Search criteria included oxidation of methionine (+15.995 Da), acetylation of the protein N-terminus (+42.011 Da), methionine loss from the protein N-terminus (–131.04 Da), and methionine loss plus acetylation of the protein N-terminus (–89.03 Da) as variable modifications and carbamidomethylation of cysteine (+57.0214) and the addition of the TMTpro mass tag (+304.207) to peptide N-termini and lysine as fixed modifications. For the phosphoproteome analysis, phosphorylation of serine, threonine, and tyrosine (+79.966) was also included as a variable modification. Searches were performed with full tryptic digestion and a maximum of two missed cleavages were allowed. To ensure a high confidence in the identified phosphopeptides to the matched proteins, the reverse database search option was enabled and all data was filtered to satisfy FDR of 5%.

Phosphoproteome analysis

Phosphoproteome data was processed from a single dataset containing $\log_2$-adjusted, normalised phosphopeptide abundances. Phosphosites were retained if a residue position could be unambiguously parsed and, where available, localisation probability was ≥75%. Intensities were collapsed to one value per phosphosite by averaging across peptides mapping to the same site. Site-level quality control was performed using multiple orthogonal metrics, including missingness, inter-sample correlation, PCA distance, and distributional properties. These metrics were combined into an objective composite score used for diagnostic purposes only; no samples were excluded a priori.

Differential phosphorylation was assessed using limma (***Ritchie et al., 2015***) with empirical Bayes moderation. Initial heatmap and PCA of the most differentially enriched phosphosites revealed a clear batch effect (likely due to one batch undergoing a freeze-thaw cycle prior to protein isolation, ***Figure 4—figure supplement 2***). Limma modelling (***Ritchie et al., 2015***) using batch as a covariate effectively controlled the effect, with samples clustering by experiment group (***Figure 4***). Genes were ranked for GSEA using the most extreme site-level moderated t-statistic per gene from a limma model, including batch as a covariate. This ranking incorporates both effect size and variance and avoids overweighting noisy phosphosites. Gene-level pathway enrichment was performed using Reactome PA (***Yu and He, 2015***; ***Yu et al., 2012***), ranking genes by site-derived t-statistic. Phosphosite-level kinase and pathway enrichment was performed using directional PTM-SEA implemented via fgsea (***Korotkevich et al., 2016***). Gene identifier mapping was performed using biomaRt (***Durinck et al., 2009***) and AnnotationDbi (***Pagès et al., 2025b***). Cross-species phosphosite mapping was performed using pairwise protein sequence alignment implemented in Biostrings using pwalign (***Pagès et al., 2025a***; ***Aboyoun and Gentlemen, 2025***). Rat phosphosites were mapped to human orthologues via gene orthology and full-length protein sequence alignment, retaining only sites with matched residues and position. Directional PTM-SEA was then performed using fgsea (***Korotkevich et al., 2016***) with site-level t-statistics as the ranking metric and PTMsigDB kinase signatures. Kinase enrichment results were visualised using volcano plots, dotplots, and heatmaps. All enrichment thresholds were treated as hypothesis-generating and are reported as such.

Statistical analysis

Descriptive statistics including mean ± standard deviation are reported in the main text. Statistical details for experiments can be found in figure legends, including n numbers, statistical test used, and level of significance. Data distributions were visually inspected and tested for normality using the Shapiro-Wilk test. All data were normally distributed. One-way analysis of variance (ANOVA) was used for multiple group comparisons, followed by Sidak's or Holm-Sidak's post hoc test to identify

significant differences as reported in the text and figure legends. There were two independent factors, viral vector construct (MPA^{EGFP} and MPA^{Gq}) and ambient environment temperature (room [21–22°C] or thermoneutral [30°C]). The dependent factors were core body temperature, heart rate, activity, and heart infarct size. Activity data was analysed using a repeated-measures ANOVA. A two-tailed paired t-test was used to analyse the oxygen consumption data to assess within animal changes, pre- and post-CNO injection. All analyses were performed using GraphPad Prism (Version 10.4.1).

Acknowledgements

We would like to thank undergraduate students Aditya Sethi and Hayaan Rizvi for their help with processing the proteomics samples and Zeynab Mohamed for her help with collecting some of the mCherry immunohistochemistry data.

Additional information

Funding

Funder	Grant reference number	Author
Wellcome Trust	10.35802/308526	Michael Ambler
Medical Research Council	MR/W029138/1	Anthony E Pickering Michael Ambler
Biotechnology and Biological Sciences Research Council	BB/W007266/1	Megan Elley Timna Hitrec Anthony E Pickering Michael Thomas Ambler

The funders had no role in study design, data collection and interpretation, or the decision to submit the work for publication. For the purpose of Open Access, the authors have applied a CC BY public copyright license to any Author Accepted Manuscript version arising from this submission.

Author contributions

Megan Elley, Conceptualization, Formal analysis, Investigation, Visualization, Methodology, Writing – original draft, Writing – review and editing; Ludovico Taddei, Conceptualization, Formal analysis, Investigation, Methodology, Writing – review and editing; Muzammil Ali Khan, Una R Wilcox, Formal analysis, Investigation; Timna Hitrec, Conceptualization, Formal analysis, Investigation, Writing – review and editing; Martin Lewis, Conceptualization, Methodology; Anthony E Pickering, Conceptualization, Formal analysis, Supervision, Writing – review and editing; Michael Ambler, Conceptualization, Formal analysis, Supervision, Visualization, Methodology, Writing – original draft, Writing – review and editing

Author ORCIDs

Megan Elley https://orcid.org/0009-0006-2397-4301
Ludovico Taddei https://orcid.org/0000-0002-6405-8119
Muzammil Ali Khan https://orcid.org/0000-0003-2474-1076
Anthony E Pickering https://orcid.org/0000-0003-0345-0456
Michael Ambler https://orcid.org/0000-0001-7884-6522

Ethics

All studies had the approval of the local University of Bristol Animal Welfare and Ethical Review Board 376 and were conducted in accordance with the UK animals (scientific procedures) act under Home Office Project Licence number PP3581754.

Peer review material

Version of Record:
Reviewer #1 (Public review): https://doi.org/10.7554/eLife.110559.3.sa1
Reviewer #2 (Public review): https://doi.org/10.7554/eLife.110559.3.sa2
Reviewer #3 (Public review): https://doi.org/10.7554/eLife.110559.3.sa3

Reviewer #4 (Public review): https://doi.org/10.7554/eLife.110559.3.sa4
Author response https://doi.org/10.7554/eLife.110559.3.sa5

Reviewed preprint v2
Reviewer #1 (Public review): https://doi.org/10.7554/eLife.110559.2.sa4
Reviewer #2 (Public review): https://doi.org/10.7554/eLife.110559.2.sa3
Reviewer #3 (Public review): https://doi.org/10.7554/eLife.110559.2.sa2
Reviewer #4 (Public review): https://doi.org/10.7554/eLife.110559.2.sa1
Author response: https://doi.org/10.7554/eLife.110559.2.sa0
eLife Assessment https://doi.org/10.7554/eLife.110559.2.sa5

Reviewed preprint v1
Reviewer #1 (Public review): https://doi.org/10.7554/eLife.110559.1.sa2
Reviewer #2 (Public review): https://doi.org/10.7554/eLife.110559.1.sa1
Reviewer #3 (Public review): https://doi.org/10.7554/eLife.110559.1.sa0
eLife Assessment https://doi.org/10.7554/eLife.110559.1.sa3

Additional files

Supplementary files
MDAR checklist

Data availability
Phosphoproteome data alongside analysis scripts were deposited here: https://doi.org/10.5061/dryad.v6wwpzh9r.

The following dataset was generated:

Author(s)	Year	Dataset title	Dataset URL	Database and Identifier
Elley M, Taddei L, Khan M, Wilcox UR, Hitrec T, Pickering AE, Ambler MT	2026	Data from: Synthetic torpor in the rat protects the heart from ischaemia-reperfusion injury	https://doi.org/10.5061/dryad.v6wwpzh9r	Dryad Digital Repository, 10.5061/dryad.v6wwpzh9r

References

Aboyoun P, Gentlemen R. 2025. Pwalign: perform pairwise sequence alignments. v1.4.0. Bioconductor. https://doi.org/10.18129/B9.bioc.pwalign

Alföldi P, Rubicsek G, Cserni G, Obál F. 1990. Brain and core temperatures and peripheral vasomotion during sleep and wakefulness at various ambient temperatures in the rat. *Pflügers Archiv* **417**:336–341. DOI: https://doi.org/10.1007/BF00371001, PMID: 2274418

Ambler M, Hitrec T, Pickering A. 2021. Turn it off and on again: characteristics and control of torpor. *Wellcome Open Research* **6**:313. DOI: https://doi.org/10.12688/wellcomeopenres.17379.2, PMID: 35087956

Ambler M, Hitrec T, Wilson A, Cerri M, Pickering A. 2022. Neurons in the dorsomedial hypothalamus promote, prolong, and deepen torpor in the mouse. *The Journal of Neuroscience* **42**:4267–4277. DOI: https://doi.org/10.1523/JNEUROSCI.2102-21.2022, PMID: 35440490

Armbruster BN, Li X, Pausch MH, Herlitze S, Roth BL. 2007. Evolving the lock to fit the key to create a family of G protein-coupled receptors potently activated by an inert ligand. *PNAS* **104**:5163–5168. DOI: https://doi.org/10.1073/pnas.0700293104, PMID: 17360345

Barnes BM, Carey HV. 2004. *Life in the Cold: Evolution, Mechanisms, Adaptation, and Application*. Institute of Arctic Biology, University of Alaska Fairbanks.

Basu K, Gravel C, Tomioka R, Kaneko T, Tamamaki N, Sík A. 2008. Novel strategy to selectively label excitatory and inhibitory neurons in the cerebral cortex of mice. *Journal of Neuroscience Methods* **170**:212–219. DOI: https://doi.org/10.1016/j.jneumeth.2008.01.016, PMID: 18321591

Bell RM, Mocanu MM, Yellon DM. 2011. Retrograde heart perfusion: the Langendorff technique of isolated heart perfusion. *Journal of Molecular and Cellular Cardiology* **50**:940–950. DOI: https://doi.org/10.1016/j.yjmcc.2011.02.018, PMID: 21385587

Bertero E, Popoiu TA, Maack C. 2024. Mitochondrial calcium in cardiac ischemia/reperfusion injury and cardioprotection. *Basic Research in Cardiology* **119**:569–585. DOI: https://doi.org/10.1007/s00395-024-01060-2, PMID: 38890208

Bhowmick S, Moore JT, Kirschner DL, Drew KL. 2017. Arctic ground squirrel hippocampus tolerates oxygen glucose deprivation independent of hibernation season even when not hibernating and after ATP depletion, acidosis, and glutamate efflux. *Journal of Neurochemistry* **142**:160–170. DOI: https://doi.org/10.1111/jnc.13996, PMID: 28222226

Bolling SF, Tramontini NL, Kilgore KS, Su TP, Oeltgen PR, Harlow HH, Oeltgen PR. 1997. Use of "natural" hibernation induction triggers for myocardial protection. *The Annals of Thoracic Surgery* **64**:623–627. DOI: https://doi.org/10.1016/s0003-4975(97)00631-0, PMID: 9307448

Borgo C, D'Amore C, Sarno S, Salvi M, Ruzzene M. 2021. Protein kinase CK2: a potential therapeutic target for diverse human diseases. *Signal Transduction and Targeted Therapy* **6**:183. DOI: https://doi.org/10.1038/s41392-021-00567-7, PMID: 33994545

Brauch KM, Dhruv ND, Hanse EA, Andrews MT. 2005. Digital transcriptome analysis indicates adaptive mechanisms in the heart of a hibernating mammal. *Physiological Genomics* **23**:227–234. DOI: https://doi.org/10.1152/physiolgenomics.00076.2005, PMID: 16076930

Cerri M, Mastrotto M, Tupone D, Martelli D, Luppi M, Perez E, Zamboni G, Amici R. 2013. The inhibition of neurons in the central nervous pathways for thermoregulatory cold defense induces a suspended animation state in the rat. *The Journal of Neuroscience* **33**:2984–2993. DOI: https://doi.org/10.1523/JNEUROSCI.3596-12.2013, PMID: 23407956

Cerri M. 2017. The central control of energy expenditure: exploiting torpor for medical applications. *Annual Review of Physiology* **79**:167–186. DOI: https://doi.org/10.1146/annurev-physiol-022516-034133, PMID: 27813827

Chang H, Peng X, Yan X, Zhang J, Xu S, Wang H, Wang Z, Ma X, Gao Y. 2020. Autophagy and Akt-mTOR signaling display periodic oscillations during torpor-arousal cycles in oxidative skeletal muscle of Daurian ground squirrels (Spermophilus dauricus). *Journal of Comparative Physiology. B, Biochemical, Systemic, and Environmental Physiology* **190**:113–123. DOI: https://doi.org/10.1007/s00360-019-01245-5, PMID: 31729534

Childers CL, Tessier SN, Storey KB. 2019. The heart of a hibernator: EGFR and MAPK signaling in cardiac muscle during the hibernation of thirteen-lined ground squirrels, *Ictidomys tridecemlineatus*. *PeerJ* **7**:e7587. DOI: https://doi.org/10.7717/peerj.7587, PMID: 31534849

Chu S-J, Perng W-C, Hung C-M, Chang D-M, Lin S-H, Huang K-L. 2005. Effects of various body temperatures after lipopolysaccharide-induced lung injury in rats. *Chest* **128**:327–336. DOI: https://doi.org/10.1378/chest.128.1.327, PMID: 16002954

Dankiewicz J, Cronberg T, Lilja G, Jakobsen JC, Levin H, Ullén S, Rylander C, Wise MP, Oddo M, Cariou A, Bělohlávek J, Hovdenes J, Saxena M, Kirkegaard H, Young PJ, Pelosi P, Storm C, Taccone FS, Joannidis M, Callaway C, et al. 2021. Hypothermia versus normothermia after out-of-hospital cardiac arrest. *The New England Journal of Medicine* **384**:2283–2294. DOI: https://doi.org/10.1056/NEJMoa2100591, PMID: 34133859

Das A, Salloum FN, Durrant D, Ockaili R, Kukreja RC. 2012. Rapamycin protects against myocardial ischemia-reperfusion injury through JAK2-STAT3 signaling pathway. *Journal of Molecular and Cellular Cardiology* **53**:858–869. DOI: https://doi.org/10.1016/j.yjmcc.2012.09.007, PMID: 22999860

Delgado-Betancourt V, Chinda K, Mesirca P, Barrère C, Covinhes A, Gallot L, Vincent A, Bidaud I, Kumphune S, Nargeot J, Piot C, Wickman K, Mangoni ME, Barrère-Lemaire S. 2023. Heart rate reduction after genetic ablation of L-type $Ca_v1.3$ channels induces cardioprotection against ischemia-reperfusion injury. *Frontiers in Cardiovascular Medicine* **10**:1134503. DOI: https://doi.org/10.3389/fcvm.2023.1134503, PMID: 37593151

Duan Q, Yang W, Zhu X, Feng Z, Song J, Xu X, Kong M, Mao J, Shen J, Deng Y, Tao R, Xu H, Chen W, Li W, Dong A, Han J. 2024. Deptor protects against myocardial ischemia-reperfusion injury by regulating the mTOR signaling and autophagy. *Cell Death Discovery* **10**:508. DOI: https://doi.org/10.1038/s41420-024-02263-1, PMID: 39702468

Dundee JW, Gray TC, Mesham PR, Scott WE. 1953. Hypothermia with autonomic block in man. *British Medical Journal* **2**:1237–1243. DOI: https://doi.org/10.1136/bmj.2.4848.1237, PMID: 13106394

Durinck S, Spellman PT, Birney E, Huber W. 2009. Mapping identifiers for the integration of genomic datasets with the R/Bioconductor package biomaRt. *Nature Protocols* **4**:1184–1191. DOI: https://doi.org/10.1038/nprot.2009.97, PMID: 19617889

Eddy SF, Storey KB. 2007. p38 MAPK regulation of transcription factor targets in muscle and heart of the hibernating bat, Myotis lucifugus. *Cell Biochemistry and Function* **25**:759–765. DOI: https://doi.org/10.1002/cbf.1416, PMID: 17487931

Egashira Y, Mori Y, Yanagawa Y, Takamori S. 2018. Development of lentiviral vectors for efficient glutamatergic-selective gene expression in cultured hippocampal neurons. *Scientific Reports* **8**:15156. DOI: https://doi.org/10.1038/s41598-018-33509-5, PMID: 30310105

Faherty SL, Villanueva-Cañas JL, Klopfer PH, Albà MM, Yoder AD. 2016. Gene expression profiling in the hibernating primate, cheirogaleus medius. *Genome Biology and Evolution* **8**:2413–2426. DOI: https://doi.org/10.1093/gbe/evw163, PMID: 27412611

Ferhat L, Soussi R, Masse M, Kyriatzis G, Girard S, Gassiot F, Gaudin N, Laurencin M, Bernard A, Bôle A, Ferracci G, Smirnova M, Roman F, Dive V, Cisternino S, Temsamani J, David M, Lécorché P, Jacquot G, Khrestchatisky M. 2025. A peptide-neurotensin conjugate that crosses the blood-brain barrier induces pharmacological hypothermia associated with anticonvulsant, neuroprotective, and anti-inflammatory properties following status epilepticus in mice. *eLife* **13**:RP100527. DOI: https://doi.org/10.7554/eLife.100527, PMID: 40152901

Fishbein MC, Meerbaum S, Rit J, Lando U, Kanmatsuse K, Mercier JC, Corday E, Ganz W. 1981. Early phase acute myocardial infarct size quantification: Validation of the triphenyl tetrazolium chloride tissue enzyme staining technique. *American Heart Journal* **101**:593–600. DOI: https://doi.org/10.1016/0002-8703(81)90226-X

Ham DJ, Börsch A, Chojnowska K, Lin S, Leuchtmann AB, Ham AS, Thürkauf M, Delezie J, Furrer R, Burri D, Sinnreich M, Handschin C, Tintignac LA, Zavolan M, Mittal N, Rüegg MA. 2025. Distinct and additive effects of calorie restriction and rapamycin in aging skeletal muscle. *Nature Communications* **13**:2025. DOI: https://doi.org/10.1038/s41467-022-29714-6, PMID: 35440545

Harding EC, Yu X, Miao A, Andrews N, Ma Y, Ye Z, Lignos L, Miracca G, Ba W, Yustos R, Vyssotski AL, Wisden W, Franks NP. 2018. A neuronal hub binding sleep initiation and body cooling in response to a warm external stimulus. *Current Biology* **28**:2263–2273. DOI: https://doi.org/10.1016/j.cub.2018.05.054, PMID: 30017485

Haykin H, Avishai E, Krot M, Ghiringhelli M, Reshef M, Abboud Y, Melamed S, Merom S, Boshnak N, Azulay-Debby H, Ziv T, Gepstein L, Rolls A. 2024. Reward system activation improves recovery from acute myocardial infarction. *Nature Cardiovascular Research* **3**:841–856. DOI: https://doi.org/10.1038/s44161-024-00491-3, PMID: 39196183

Heldmaier G, Ortmann S, Elvert R. 2004. Natural hypometabolism during hibernation and daily torpor in mammals. *Respiratory Physiology & Neurobiology* **141**:317–329. DOI: https://doi.org/10.1016/j.resp.2004.03.014, PMID: 15288602

Heldmaier G, Braulke L, Flick J, Ruf T. 2024. Multiple ultradian rhythms of metabolism, body temperature and activity in Djungarian hamsters. *Journal of Comparative Physiology B* **194**:501–518. DOI: https://doi.org/10.1007/s00360-024-01569-x, PMID: 38967807

Herzig S, Shaw RJ. 2018. AMPK: guardian of metabolism and mitochondrial homeostasis. *Nature Reviews. Molecular Cell Biology* **19**:121–135. DOI: https://doi.org/10.1038/nrm.2017.95, PMID: 28974774

Hrvatin S, Sun S, Wilcox OF, Yao H, Lavin-Peter AJ, Cicconet M, Assad EG, Palmer ME, Aronson S, Banks AS, Griffith EC, Greenberg ME. 2020. Neurons that regulate mouse torpor. *Nature* **583**:115–121. DOI: https://doi.org/10.1038/s41586-020-2387-5, PMID: 32528180

Huang YG, Flaherty SJ, Pothecary CA, Foster RG, Peirson SN, Vyazovskiy VV. 2021. The relationship between fasting-induced torpor, sleep, and wakefulness in laboratory mice. *SLEEP* **44**:zsab093. DOI: https://doi.org/10.1093/sleep/zsab093, PMID: 33838033

Jani A, Epperson E, Martin J, Pacic A, Ljubanovic D, Martin SL, Edelstein CL. 2011. Renal protection from prolonged cold ischemia and warm reperfusion in hibernating squirrels. *Transplantation* **92**:1215–1221. DOI: https://doi.org/10.1097/TP.0b013e3182366401, PMID: 22082817

Korotkevich G, Sukhov V, Budin N, Shpak B, Artyomov MN, Sergushichev A. 2016 Fast gene set enrichment analysis. *bioRxiv*. DOI: https://doi.org/10.1101/060012

Kuczynski AM, Demchuk AM, Almekhlafi MA. 2019. Therapeutic hypothermia: Applications in adults with acute ischemic stroke. *Brain Circulation* **5**:43–54. DOI: https://doi.org/10.4103/bc.bc_5_19, PMID: 31334356

Kurtz CC, Lindell SL, Mangino MJ, Carey HV. 2006. Hibernation confers resistance to intestinal ischemia-reperfusion injury. *American Journal of Physiology. Gastrointestinal and Liver Physiology* **291**:G895–G901. DOI: https://doi.org/10.1152/ajpgi.00155.2006, PMID: 16751173

Kyo S, Murata K, Kawatou M, Minatoya K, Sunagawa GA, Masumoto H. 2022. Quiescence-inducing neurons-induced hypometabolism ameliorates acute kidney injury in a mouse model mimicking cardiovascular surgery requiring circulatory arrest. *JTCVS Open* **12**:201–210. DOI: https://doi.org/10.1016/j.xjon.2022.11.001, PMID: 36590714

Leonov Y, Sterz F, Safar P, Radovsky A, Oku K, Tisherman S, Stezoski SW. 1990. Mild cerebral hypothermia during and after cardiac arrest improves neurologic outcome in dogs. *Journal of Cerebral Blood Flow and Metabolism* **10**:57–70. DOI: https://doi.org/10.1038/jcbfm.1990.8, PMID: 2298837

Machado NLS, Bandaru SS, Abbott SBG, Saper CB. 2020. EP3R-expressing glutamatergic preoptic neurons mediate inflammatory fever. *The Journal of Neuroscience* **40**:2573–2588. DOI: https://doi.org/10.1523/JNEUROSCI.2887-19.2020, PMID: 32079648

Machhada A, Hosford PS, Dyson A, Ackland GL, Mastitskaya S, Gourine AV. 2020. Optogenetic stimulation of vagal efferent activity preserves left ventricular function in experimental heart failure. *JACC. Basic to Translational Science* **5**:799–810. DOI: https://doi.org/10.1016/j.jacbts.2020.06.002, PMID: 32875170

Marshall CJ, Pickering AE, Ambler MT. 2026. Estrous cycle modulates fasting-induced torpor propensity via hypothalamic estrogen signalling. *Scientific Reports* **16**:11214. DOI: https://doi.org/10.1038/s41598-026-41051-y, PMID: 41760784

Mastitskaya S, Marina N, Gourine A, Gilbey MP, Spyer KM, Teschemacher AG, Kasparov S, Trapp S, Ackland GL, Gourine AV. 2012. Cardioprotection evoked by remote ischaemic preconditioning is critically dependent on the activity of vagal pre-ganglionic neurones. *Cardiovascular Research* **95**:487–494. DOI: https://doi.org/10.1093/cvr/cvs212, PMID: 22739118

Moffitt JR, Bambah-Mukku D, Eichhorn SW, Vaughn E, Shekhar K, Perez JD, Rubinstein ND, Hao J, Regev A, Dulac C, Zhuang X. 2018. Molecular, spatial, and functional single-cell profiling of the hypothalamic preoptic region. *Science* **362**:eaau5324. DOI: https://doi.org/10.1126/science.aau5324, PMID: 30385464

Murray CJL, Aravkin AY, Zheng P, Abbafati C, Abbas KM, Abbasi-Kangevari M, Abd-Allah F, Abdelalim A, Abdollahi M, Abdollahpour I, Abegaz KH, Abolhassani H, Aboyans V, Abreu LG, Abrigo MRM, Abualhasan A, Abu-Raddad LJ, Abushouk AI, Adabi M, Adekanmbi V, et al. 2020. Global burden of 87 risk factors in 204 countries and territories, 1990–2019: a systematic analysis for the global burden of disease study 2019. *The Lancet* **396**:1223–1249. DOI: https://doi.org/10.1016/S0140-6736(20)30752-2, PMID: 33069327

Muslin AJ. 2008. MAPK signalling in cardiovascular health and disease: molecular mechanisms and therapeutic targets. *Clinical Science* **115**:203–218. DOI: https://doi.org/10.1042/CS20070430, PMID: 18752467

Nakamura Y, Yahiro T, Fukushima A, Kataoka N, Hioki H, Nakamura K. 2022. Prostaglandin EP3 receptor-expressing preoptic neurons bidirectionally control body temperature via tonic GABAergic signaling. *Science Advances* **8**:eadd5463. DOI: https://doi.org/10.1126/sciadv.add5463, PMID: 36563142

Nielsen N, Wetterslev J, Cronberg T, Erlinge D, Gasche Y, Hassager C, Horn J, Hovdenes J, Kjaergaard J, Kuiper M, Pellis T, Stammet P, Wanscher M, Wise MP, Åneman A, Al-Subaie N, Boesgaard S, Bro-Jeppesen J, Brunetti I, Bugge JF, et al. 2013. Targeted temperature management at 33°C versus 36°C after cardiac arrest. *The New England Journal of Medicine* **369**:2197–2206. DOI: https://doi.org/10.1056/NEJMoa1310519, PMID: 24237006

Ottem EN, Godwin JG, Krishnan S, Petersen SL. 2004. Dual-phenotype GABA/glutamate neurons in adult preoptic area: sexual dimorphism and function. *The Journal of Neuroscience* **24**:8097–8105. DOI: https://doi.org/10.1523/JNEUROSCI.2267-04.2004, PMID: 15371511

Padilla SL, Johnson CW, Barker FD, Patterson MA, Palmiter RD. 2018. A neural circuit underlying the generation of hot flushes. *Cell Reports* **24**:271–277. DOI: https://doi.org/10.1016/j.celrep.2018.06.037, PMID: 29996088

Pagès H, Aboyoun P, Gentleman R, DebRoy S. 2025a. Biostrings: efficient manipulation of biological strings. v2.76.0. Bioconductor. https://doi.org/10.18129/B9.bioc.Biostrings

Pagès H, Carlson M, Falcon S, Li N. 2025b. AnnotationDbi: manipulation of sqlite-based annotations in bioconductor. v1.70.0. Bioconductor. https://doi.org/10.18129/B9.bioc.AnnotationDbi

Ritchie ME, Phipson B, Wu D, Hu Y, Law CW, Shi W, Smyth GK. 2015. limma powers differential expression analyses for RNA-sequencing and microarray studies. *Nucleic Acids Research* **43**:e47. DOI: https://doi.org/10.1093/nar/gkv007, PMID: 25605792

Roth BL. 2016. DREADDs for neuroscientists. *Neuron* **89**:683–694. DOI: https://doi.org/10.1016/j.neuron.2016.01.040, PMID: 26889809

Sandestig A, Romner B, Grände PO. 2014. Therapeutic hypothermia in children and adults with severe traumatic brain injury. *Therapeutic Hypothermia and Temperature Management* **4**:10–20. DOI: https://doi.org/10.1089/ther.2013.0024, PMID: 24660099

Saper CB, Machado NLS. 2020. Flipping the switch on the body's thermoregulatory system. *Nature* **583**:34–35. DOI: https://doi.org/10.1038/d41586-020-01600-5, PMID: 32601488

Saxton RA, Sabatini DM. 2017. mTOR signaling in growth, metabolism, and disease. *Cell* **168**:960–976. DOI: https://doi.org/10.1016/j.cell.2017.02.004, PMID: 28283069

Shahid M, Spagnolli E, Ernande L, Thoonen R, Kolodziej SA, Leyton PA, Cheng J, Tainsh RET, Mayeur C, Rhee DK, Wu MX, Scherrer-Crosbie M, Buys ES, Zapol WM, Bloch KD, Bloch DB. 2016. BMP type I receptor ALK2 is required for angiotensin II-induced cardiac hypertrophy. *American Journal of Physiology. Heart and Circulatory Physiology* **310**:H984–H994. DOI: https://doi.org/10.1152/ajpheart.00879.2015, PMID: 26873969

Srere HK, Wang LC, Martin SL. 1992. Central role for differential gene expression in mammalian hibernation. *PNAS* **89**:7119–7123. DOI: https://doi.org/10.1073/pnas.89.15.7119, PMID: 1379733

Swaminathan PD, Purohit A, Hund TJ, Anderson ME. 2012. CaMKII: linking heart failure and arrhythmias. *Circulation Research* **110**:1661–1677. DOI: https://doi.org/10.1161/CIRCRESAHA.111.243956, PMID: 22679140

Swoap SJ, Gutilla MJ. 2009. Cardiovascular changes during daily torpor in the laboratory mouse. *American Journal of Physiology. Regulatory, Integrative and Comparative Physiology* **297**:R769–R774. DOI: https://doi.org/10.1152/ajpregu.00131.2009, PMID: 19587115

Takahashi TM, Sunagawa GA, Soya S, Abe M, Sakurai K, Ishikawa K, Yanagisawa M, Hama H, Hasegawa E, Miyawaki A, Sakimura K, Takahashi M, Sakurai T. 2020. A discrete neuronal circuit induces a hibernation-like state in rodents. *Nature* **583**:109–114. DOI: https://doi.org/10.1038/s41586-020-2163-6, PMID: 32528181

Upton BA, D'Souza SP, Lang RA. 2021. QPLOT neurons-converging on a thermoregulatory preoptic neuronal population. *Frontiers in Neuroscience* **15**:665762. DOI: https://doi.org/10.3389/fnins.2021.665762, PMID: 34017237

Veres JM, Andrasi T, Nagy-Pal P, Hajos N. 2023. CaMKIIα promoter-controlled circuit manipulations target both pyramidal cells and inhibitory interneurons in cortical networks. *eNeuro* **10**:ENEURO.0070-23.2023. DOI: https://doi.org/10.1523/ENEURO.0070-23.2023, PMID: 36963833

Virani SS, Alonso A, Aparicio HJ, Benjamin EJ, Bittencourt MS, Callaway CW, Carson AP, Chamberlain AM, Cheng S, Delling FN, Elkind MSV, Evenson KR, Ferguson JF, Gupta DK, Khan SS, Kissela BM, Knutson KL, Lee CD, Lewis TT, Liu J, et al. 2021. Heart disease and stroke statistics-2021 update: a report from the american heart association. *Circulation* **143**:e254–e743. DOI: https://doi.org/10.1161/CIR.0000000000000950, PMID: 33501848

Wheatley WSR, Marshall CJ, Taddei L, Hitrec T, Pickering AE, Ambler MT. 2025. The cold truth: torpor as a confound in studies of caloric restriction. *Journal of Comparative Physiology. B, Biochemical, Systemic, and Environmental Physiology* **195**:263–276. DOI: https://doi.org/10.1007/s00360-025-01616-1, PMID: 40488879

Worp HB, Macleod MR, Kollmar R. 2010. for the european stroke research network for hypothermia (EuroHYP). therapeutic hypothermia for acute ischemic stroke: ready to start large randomized trials. *Journal of Cerebral Blood Flow and Metabolism* **30**:1079–1093. DOI: https://doi.org/10.1038/jcbfm.2010.44, PMID: 20354545

Wu CW, Storey KB. 2012. Regulation of the mTOR signaling network in hibernating thirteen-lined ground squirrels. *The Journal of Experimental Biology* **215**:1720–1727. DOI: https://doi.org/10.1242/jeb.066225, PMID: 22539739

Xie LH, Gwathmey JK, Zhao Z. 2021. Cardiac adaptation and cardioprotection against arrhythmias and ischemia-reperfusion injury in mammalian hibernators. *Pflugers Archiv* **473**:407–416. DOI: https://doi.org/10.1007/s00424-020-02511-0, PMID: 33394082

Yu G, Wang LG, Han Y, He QY. 2012. clusterProfiler: an R package for comparing biological themes among gene clusters. *OMICS* **16**:284–287. DOI: https://doi.org/10.1089/omi.2011.0118, PMID: 22455463

Yu G, He QY. 2015. ReactomePA: an R/Bioconductor package for reactome pathway analysis and visualization. *Molecular BioSystems* **12**:477–479. DOI: https://doi.org/10.1039/C5MB00663E, PMID: 26661513

Yu S, Qualls-Creekmore E, Rezai-Zadeh K, Jiang Y, Berthoud HR, Morrison CD, Derbenev AV, Zsombok A, Münzberg H. 2016. Glutamatergic preoptic area neurons that express leptin receptors drive temperature-dependent body weight homeostasis. *The Journal of Neuroscience* **36**:5034–5046. DOI: https://doi.org/10.1523/JNEUROSCI.0213-16.2016, PMID: 27147656

Zakharova NM, Tarahovsky YS, Fadeeva IS, Komelina NP, Khrenov MO, Glushkova OV, Prokhorov DA, Kutyshenko VP, Kovtun AL. 2019. A pharmacological composition for induction of a reversible torpor-like state and hypothermia in rats. *Life Sciences* **219**:190–198. DOI: https://doi.org/10.1016/j.lfs.2019.01.023, PMID: 30658098

Zancanaro C, Malatesta M, Mannello F, Vogel P, Fakan S. 1999. The kidney during hibernation and arousal from hibernation. A natural model of organ preservation during cold ischaemia and reperfusion. *Nephrology, Dialysis, Transplantation* **14**:1982–1990. DOI: https://doi.org/10.1093/ndt/14.8.1982, PMID: 10462281

Zhang R, Khoo MSC, Wu Y, Yang Y, Grueter CE, Ni G, Price EE, Thiel W, Guatimosim S, Song LS, Madu EC, Shah AN, Vishnivetskaya TA, Atkinson JB, Gurevich VV, Salama G, Lederer WJ, Colbran RJ, Anderson ME. 2005. Calmodulin kinase II inhibition protects against structural heart disease. *Nature Medicine* **11**:409–417. DOI: https://doi.org/10.1038/nm1215, PMID: 15793582

Zhang Z, Ferretti V, Güntan İ, Moro A, Steinberg EA, Ye Z, Zecharia AY, Yu X, Vyssotski AL, Brickley SG, Yustos R, Pillidge ZE, Harding EC, Wisden W, Franks NP. 2015. Neuronal ensembles sufficient for recovery sleep and the sedative actions of α2 adrenergic agonists. *Nature Neuroscience* **18**:553–561. DOI: https://doi.org/10.1038/nn.3957, PMID: 25706476

Zhang KX, D'Souza S, Upton BA, Kernodle S, Vemaraju S, Nayak G, Gaitonde KD, Holt AL, Linne CD, Smith AN, Petts NT, Batie M, Mukherjee R, Tiwari D, Buhr ED, Van Gelder RN, Gross C, Sweeney A, Sanchez-Gurmaches J, Seeley RJ, et al. 2020a. Violet-light suppression of thermogenesis by opsin 5 hypothalamic neurons. *Nature* **585**:420–425. DOI: https://doi.org/10.1038/s41586-020-2683-0, PMID: 32879486

Zhang Z, Reis FMCV, He Y, Park JW, DiVittorio JR, Sivakumar N, van Veen JE, Maesta-Pereira S, Shum M, Nichols I, Massa MG, Anderson S, Paul K, Liesa M, Ajijola OA, Xu Y, Adhikari A, Correa SM. 2020b. Estrogen-sensitive medial preoptic area neurons coordinate torpor in mice. *Nature Communications* **11**:6378. DOI: https://doi.org/10.1038/s41467-020-20050-1, PMID: 33311503

Zhang S, Zhang X, Zhong H, Li X, Wu Y, Ju J, Liu B, Zhang Z, Yan H, Wang Y, Song K, Hou ST. 2022. Hypothermia evoked by stimulation of medial preoptic nucleus protects the brain in a mouse model of ischaemia. *Nature Communications* **13**:6890. DOI: https://doi.org/10.1038/s41467-022-34735-2, PMID: 36371436

Zhang M, Liu Q, Meng H, Duan H, Liu X, Wu J, Gao F, Wang S, Tan R, Yuan J. 2024. Ischemia-reperfusion injury: molecular mechanisms and therapeutic targets. *Signal Transduction and Targeted Therapy* **9**:12. DOI: https://doi.org/10.1038/s41392-023-01688-x, PMID: 38185705

Zhao S, Shao C, Goropashnaya AV, Stewart NC, Xu Y, Tøien Ø, Barnes BM, Fedorov VB, Yan J. 2010. Genomic analysis of expressed sequence tags in American black bear Ursus americanus. *BMC Genomics* **11**:201. DOI: https://doi.org/10.1186/1471-2164-11-201, PMID: 20338065